Title

A Consistently High-Latitude South China From 820 to 780 Ma: Implications for Exclusion From Rodinia and the Feasibility of Large-Scale True Polar Wander

Journal

Journal of Geophysical Research: Solid Earth, 126(6)

ISSN

2169-9313

Authors

Park, Yuem
Swanson-Hysell, Nicholas L
Xian, Hanbiao
et al.

Publication Date

2021-06-01

DOI

10.1029/2020jb021541

Peer reviewed

A consistently high latitude South China from 820 to 780 Ma: Implications for exclusion from Rodinia and the feasibility of large-scale true polar wander

Yuem Park[1], Nicholas L. Swanson-Hysell[1], Hanbiao Xian[2], Shihong Zhang[2], Daniel J. Condon[3], Hairuo Fu[2, 4], Francis A. Macdonald[5]

[1] Department of Earth and Planetary Science, University of California, Berkeley, CA 94720, USA

[2] State Key Laboratory of Biogeology and Environmental Geology, China University of Geosciences, Beijing 100083, China

[3] Natural Environment Research Council Isotope Geosciences Laboratory, British Geological Survey, Keyworth NG12 5GG, United Kingdom

[4] Department of Earth and Planetary Sciences, Harvard University, Cambridge, MA 02138, USA

[5] Department of Earth Science, University of California, Santa Barbara, CA 93106, USA

This article has been submitted to JGR: Solid Earth

ABSTRACT

The Tonian supercontinent Rodinia is hypothesized to have included almost all Proterozoic continental blocks. Competing models variably place South China at the core or periphery of Rodinia, or separated from it entirely. Tonian paleogeographic models also vary in whether they incorporate hypothesized large and rapid oscillatory true polar wander associated with the ca. 810–795 Ma Bitter Springs Stage. Here we present paleomagnetic data paired with U-Pb CA-ID-TIMS zircon geochronology from the Tonian Xiajiang Group in South China to establish the craton's position and test the Bitter Springs Stage true polar wander hypothesis. Fine-grained siliciclastic sediments and ashes of the Xiajiang Group post-date the Jiangnan Orogeny, which united the Yangtze and Cathaysia blocks. A U-Pb zircon date of 815.73±0.18 Ma

from a tuff near the base of the Xiajiang Group constrains the Jiangnan Orogeny to have ended between ca. 830 and 816 Ma. The paleomagnetic and geochronologic data constrain South China to high latitudes ca. 813 Ma, and indicate a relatively stable high-latitude position from ca. 821 to 805 Ma. These high-latitude constraints either connect the craton to Rodinia along its periphery, or disconnect it from the supercontinent entirely. The difference in pole position between the pre-Bitter Springs Stage Xiajiang Group pole and the syn-Bitter Springs Stage Madiyi Formation pole is significantly less than that predicted for the Bitter Springs Stage true polar wander hypothesis. If this pole difference is interpreted as true polar wander superimposed upon differential plate motion, it requires South China to have been separate from Rodinia.

INTRODUCTION

Earth's lithosphere moves through two fundamental mechanisms. The more familiar of these mechanisms are tectonic motions — that is, differential movement between lithospheric plates. The second mechanism is the rotation of the entire silicate Earth in order to maintain rotational equilibrium. On any rotating planetary body, changes in the distribution of mass on (e.g. the melting of ice sheets; Mitrovica et al., 2005; Matsuyama et al., 2010; Cambiotti et al., 2010) or within (e.g. mantle convection; Spada et al., 1992) can cause reorientation of the planetary surface relative to the rotational axis (Evans, 2003; Matsuyama et al., 2014). Such reorientation causes all of Earth's tectonic plates, as well as the underlying mantle, to rotate in unison relative to the spin axis and the core. To an observer on Earth's surface, it would appear that the pole is changing position and the process is therefore referred to as true polar wander (TPW). Differential plate tectonics and TPW are operating today and were in Earth's past. Both processes are built into paleogeographic models over the past 400 million years (m.y.), with an overall dominance of differential plate tectonics (Steinberger and Torsvik, 2008; Torsvik et al., 2012).

Plate kinematic reconstructions indicate that the median plate velocity over the past 200 m.y., during which a seafloor spreading record is preserved, is ∼4 cm/yr (Zahirovic et al., 2015).

Although plate velocities have been observed to significantly exceed this median value, such as during the rapid northward motion of India toward Eurasia ca. 55 Ma when its velocity was as high as 19 cm/yr (van Hinsbergen et al., 2011; Zahirovic et al., 2012), such motions are short-lived (up to ∼10 m.y.; Zahirovic et al., 2015). Based on these plate kinematic reconstructions, it has been argued that plate velocities rarely exceed ∼20 cm/yr (Meert et al., 1993; Zahirovic et al., 2015).

Over the past 300 m.y., there has been near continuous TPW at rates of 1–10 cm/yr attributed to advection of mass heterogeneities in the mantle (Steinberger and Torsvik, 2008; Torsvik et al., 2012), with the possibility of more rapid TPW in the Jurassic (Kent et al., 2015). These rates are comparable to rates of differential plate motion, which can make TPW difficult to distinguish in the record. While it is a matter of contention (Tsai and Stevenson, 2007), it has been considered theoretically possible for TPW to occur at rates exceeding those of typical plate tectonics (Gold, 1955; Fisher, 1974; Steinberger and O'Connell, 1997; Evans, 2003). TPW has therefore been proposed as an explanation for large rapid shifts in paleomagnetic poles in the geological record (e.g. Kirschvink, 1997). The rate at which true polar wander can occur is a function of the magnitude of the perturbation to Earth's moment of inertia tensor, the timescale over which that perturbation is applied, and the timescale for viscoelastic adjustment of Earth's rotational bulge, which is itself largely a function of mantle viscosity (Tsai and Stevenson, 2007; Steinberger and Torsvik, 2010; Creveling et al., 2012). Additionally, stabilization is thought to result from TPW-induced stresses in the lithosphere that can form a remanent bulge (Ricard et al., 1993; Chan et al., 2014). Numerical models have suggested that velocities due to TPW motion can be higher than ∼150 cm/yr (Spada et al., 1992), although other treatments have argued that TPW exceeding ∼25 cm/yr is unlikely (Tsai and Stevenson, 2007). Ultimately, however, the rate at which TPW has proceeded at different periods of Earth history is a question for geologic and paleomagnetic records.

A pair of oscillatory TPW events ca. 810 and 795 Ma have been proposed to have occurred

during the Tonian Period of the Neoproterozoic Era (Maloof et al., 2006). This hypothesis is based on paleomagnetic, isotopic, and stratigraphic data from carbonate strata in the Akademikerbreen Group of East Svalbard — a terrane that was part of Laurentia in the Tonian (Maloof et al., 2006). Two >50° shifts in paleomagnetic direction from East Svalbard, with associated plate velocities implied to be >50 cm/yr based on an interpretation that the directions are primary, were observed to be coincident with abrupt shifts in δ^{13}C (referred to as the Bitter Springs Stage; Maloof et al., 2006). These poles are from carbonate units that are separated by unconformities that were interpreted to reflect the transient changes in local relative sea level predicted to occur given the differential response of the fluid and solid Earth (Mound et al., 1999; Maloof et al., 2006). These shifts were interpreted as 'there and back again' TPW rotations in which the entire solid Earth (and therefore all of Rodinia) rotated 50° about an equatorial axis and then returned to near its prior position (Maloof et al., 2006). Further geochronologic constraints on δ^{13}C records correlated to the Bitter Springs Stage, and therefore the proposed oscillatory TPW, constrain it to have started after 811.51±0.25 Ma (U-Pb CA-ID-TIMS zircon from a tuff ∼50 m below carbonates that record the first abrupt shift to negative δ^{13}C values in the Fifteenmile Group of northwest Canada; Macdonald et al., 2010) and to have ended by 788.72±0.24 Ma (U-Pb CA-ID-TIMS zircon from a tuff ∼250 m above carbonates that record the second abrupt shift to positive δ^{13}C values in the Tambien Group of northern Ethiopia; Swanson-Hysell et al., 2015; Park et al., 2020). Interpolation using these and other geochronologic constraints suggest that the Bitter Springs Stage started before 807.9±0.2 Ma and ended after 800.6±0.2 Ma (Swanson-Hysell et al., 2015). However, no direct geochronologic constraints exist on the Akademikerbreen Group stratigraphy, and therefore the ages of these paleomagnetic poles for Svalbard are reliant on carbon and strontium isotope chemostratigraphic correlations (Halverson et al., 2007).

Given that TPW results in rotation of the entire lithosphere around the spin axis, it should manifest in the paleomagnetic record as simultaneous motion of paleomagnetic poles across all continents, once standard differential plate tectonic motion has been subtracted out (Evans, 2003). Efforts to test the Bitter Springs Stage TPW hypothesis within the Bitter Springs Group

of central Australia led to distinct paleomagnetic pole positions from syn-Bitter Springs Stage and post-Bitter Springs Stage sedimentary rocks (Swanson-Hysell et al., 2012). The post-Bitter Springs Stage pole was developed from a hematite remanence held in Johnny's Creek Formation siltstone and is included as a constraint for Australia in models of Rodinia (e.g. Merdith et al., 2017). The syn-Bitter Springs Stage pole from Love's Creek Formation carbonate overlaps with the Cambrian apparent polar wander path of Australia, raising the possibility that the difference in position between the Love's Creek and Johnny's Creek poles is the result of remagnetization, leaving ambiguity in using these data to test the TPW hypothesis (Swanson-Hysell et al., 2012). The paleomagnetic remanence of carbonate rocks can be challenging to interpret as they are prone to remagnetization (Van Der Voo and Torsvik, 2012; Jackson and Swanson-Hysell, 2012). Carbonate remagnetization can be particularly vexing as it can result from chemical alteration at low temperatures such as the conversion of smectite clay minerals to illite. This process can lead to the authigenic formation of magnetite at temperatures as low as 70°C (Katz et al., 1998; Tohver et al., 2008). This mechanism may explain the magnetization obtained from carbonates of the Love's Creek Formation of the Bitter Springs Group as a Cambrian overprint from authigenic magnetite formation during burial (Swanson-Hysell et al., 2012). This clay transformation mechanism, or other processes associated with fluid flow, have been invoked to explain widespread remagnetization of carbonates particularly at time periods of regional orogenesis (Van Der Voo and Torsvik, 2012). For example, at the time of the Alleghenian orogeny, North American carbonates both proximal to the orogen and hundreds of kilometers away were remagnetized through the precipitation of authigenic magnetite (McCabe and Elmore, 1989; Van Der Voo and Torsvik, 2012).

Of potential relevance to the data upon which the Bitter Springs Stage TPW hypothesis was formulated, Michalski et al. (2011) developed paleomagnetic data from metasedimentary rocks from the central terrane of Svalbard that were metamorphosed and remagnetized ca. 430 Ma during the Caledonian orogeny. The remagnetization direction in these rocks has a similar position to the pre-Bitter Springs Stage pole of the Akademikerbreen Group (lGfm from Maloof

et al., 2006), leading Michalski et al. (2011) to suggest that the pole does not record a primary magnetization, and is instead the result of remagnetization at the time of the Caledonian orogeny that effected both Central and East Svalbard. However, the post-Bitter Springs Stage pole from the Akademikerbreen Group (S4fm) passes a syn-sedimentary fold test which provides strong support for a primary remanence held by magnetite for that pole. These constraints seemingly require variable remagnetization in different units of the Akademikerbreen Group for the interpretation of Michalski et al. (2011) to be correct.

These potential complexities associated with the specter of carbonate remagnetization highlight the importance of testing the Bitter Springs Stage TPW hypothesis using other lithologies such as detrital hematite-bearing siliciclastics and igneous rocks. Tonian deposition in the Nanhua Basin of South China includes reds beds and volcanic tuffs. These units potentially span the Bitter Spring Stage and provide an opportunity to develop high quality paleomagnetic data paired with precise geochronology to test both the Bitter Springs Stage TPW hypothesis and models of the configuration of the Neoproterozoic supercontinent Rodinia.

GEOLOGIC SETTING

This study presents paleomagnetic and U-Pb chemical abrasion isotope dilution thermal ionization mass spectrometry (CA-ID-TIMS) zircon geochronologic data from the Xiajiang Group in the Fanjingshan region of Guizhou province, China (Fig. 1A). The Fanjingshan region lies within the Jiangnan orogenic belt that separates the Yangtze and Cathaysia blocks of the South China craton, and is characterized by a regional anticline that developed in the Mesozoic (Fig. 1B; Li et al., 2016a; Ma et al., 2019). At the core of the anticline is the Fanjingshan Group, dominantly composed of sandstones intruded by intermediate to ultramafic sills (Fig. 1B; Wang et al., 2014). These sills are interpreted to have formed in a subduction-related environment just prior to amalgamation of the Yangtze and Cathaysia blocks (Wang et al., 2014).

Both the sedimentary rocks and the intrusive sills of the Fanjingshan Group are folded, and are separated from the overlying Xiajiang Group by an angular unconformity (Fig. 1B). Tuffs of the Fanjingshan Group in the Fanjingshan region have yielded U-Pb laser ablation inductively coupled plasma mass spectrometry (LA-ICP-MS) zircon dates of 851.3±4.0 Ma, 840±5 Ma, and 832.0±8.5 Ma (Wang et al., 2012; Gao et al., 2014). U-Pb LA-ICP-MS zircon dates for the mafic sills are 831±4 Ma and 827±15 Ma (Zhao et al., 2011), and U-Pb LA-ICP-MS detrital zircon dates within the sediments are as young as 849±6.5 Ma (Zhao et al., 2011). These dates constrain the exposure, folding, and erosion of the Fanjingshan Group to have been after ca. 830 Ma. A cobble to boulder conglomerate is often the lowest unit of the Xiajiang Group, before the sedimentary rocks transition into hundreds of meters of red, purple, green, and grey-blue graded beds of siltstone and fine-grained sandstone interbedded with volcanic ashes (Fig. 2). The fine-grained sandstone-siltstone interbeds locally exhibit ripple cross-stratification, which are interpreted to have formed as Bouma-C beds associated with distal turbidity currents. The presence of ∼1–5 cm volcanic ashes throughout the stratigraphy without lithic fragments indicate the presence of a nearby, but not immediately adjacent, volcanic arc. Existing U-Pb LA-ICP-MS zircon dates for tuffs of the Xiajiang Group in the Fanjingshan region of 814.0±6.3 Ma and 813.5±9.6 Ma (Gao et al., 2010, 2014) suggest deposition of Xiajiang Group began by ca. 815 Ma. Unconformably overlying the Xiajiang Group in the Fanjingshan region are glacial deposits correlated with the Cryogenian Sturtian 'Snowball Earth' glaciation (referred to locally as the Tiesi'ao Formation; Xiong et al., 2014). Geochronologic constraints from South China, Laurentia, Oman, and the Arabian-Nubian Shield indicate that onset of the Sturtian glaciation was rapid and globally synchronous within the available precision of the geochronology (Bowring et al., 2007; Macdonald et al., 2010; MacLennan et al., 2018; Lan et al., 2020). These constraints on the Sturtian glaciation constrain Xiajiang Group deposition to have ended prior to ca. 717 Ma. During our fieldwork, no continuous individual section was identified that captures both the Fanjingshan-Xiajiang Group contact and the contact between the Xiajiang Group and the Sturtian glacial deposits (Fig. 2). However, correlation of our individually measured sections

based on aligning the bounding unconformities of the Xiajiang Group and the geochronologic results suggests that the Xiajiang Group is ∼3000 m thick in this region (Fig. 2).

We note that the nomenclature of pre-Sturtian Neoproterozoic strata in South China varies in the literature. In some publications, the term the 'Banxi Group' is used to refer to any ca. 815–717 Ma sediments in South China, including those in our study area (e.g. Zhao et al., 2011; Zhang et al., 2019). In other publications, the term the 'Banxi Group' is used to refer exclusively to ca. 815–717 Ma sediments in the Hunan province, and equivalent strata in our study area in the Guizhou province is referred to as the 'Xiajiang Group' (e.g. Bureau of Geology and Mineral Resources of Guizhou Province, 1984; Wang et al., 2014; Xiong et al., 2014; Geng, 2015; Li et al., 2016b; Wang et al., 2016a; Yan et al., 2019). Further to the southeast, sedimentary rocks interpreted to correlate with the Banxi and Xiajiang Groups are referred to as the 'Danzhou Group' (Yan et al., 2019). There are similar regional nomenclature differences for the older Fanjingshan Group, which is referred to as the 'Fanjingshan Group' in our study area and is correlated with units known as the 'Lengjiaxi Group' and the 'Sibao Group' elsewhere, and the younger Tiesi'ao Formation, which is referred to as the 'Tiesi'ao Formation' in our study area and is correlated with units known as the 'Chang'an Formation' elsewhere. In this study, we follow the nomenclature most widely used for the Guizhou province, using the term Fanjingshan Group, and referring to the sediments unconformably bounded by the Fanjingshan Group and Sturtian glacial deposits in the Fanjingshan region as the Xiajiang Group.

METHODS

Paleomagnetism

Where exposure of the stratigraphy was good, sections were measured using a Jacob's staff. In cases where vegetation obscured the stratigraphy for hundreds of meters, the thickness of covered stratigraphy was estimated based on GPS measurements and local bedding orientations, leading

to the covered intervals shown in Figure 2.

Cores from the studied sedimentary rocks were collected using a gas-powered drill and a Pomeroy orienting device. Sun compass data were used for sample orientations when possible, and magnetic compass orientations were used when necessitated by cloud cover. Sample collection was organized into 'sites,' where each site consists of a set of samples that were obtained from within a few meters of stratigraphy. This grouping provides a useful organizational framework although it does not correspond to the definition of a site within the framework of the MagIC database wherein every sample in a site should be expected to record a direction from the same moment in time. In most cases, cores were collected from the least foliated purple/red siltstone of the Xiajiang Group, but when no such lithologies were present, green/grey-blue siltstones were also collected.

Thermal demagnetization and magnetic remanence measurements were conducted at UC Berkeley and the China University of Geosciences, Beijing. At the UC Berkeley Paleomagnetism Laboratory, measurements were made using a 2G Enterprises DC-SQUID superconducting rock magnetometer with an automated pick-and-place sample changer system (Kirschvink et al., 2008). Samples are brought into the measurement region with a quartz glass sample rod and is typically measured at $\sim 5 \times 10^{-12}$ Am^2. The magnetostatic shield that houses the magnetometer has magnetic fields <500 nT. Samples were progressively step-heated and thermally demagnetized in an ASC thermal specimen demagnetizer (residual fields <10 nT) after measurement of the natural remanent magnetization (NRM).

At the China University of Geosciences, Beijing, paleomagnetic analyses were conducted at the Laboratory of Paleomagnetism and Environmental Magnetism in a magnetically shielded room with a residual field of <300 nT. Magnetic remanence was measured using a 2G 755-4 K three-axis cryogenic magnetometer, and stepwise thermal demagnetizations were carried out with an ASC TD-48 or MMTDSC furnace, both of which have an internal residual field of <10 nT.

All paleomagnetic data to the measurements level, as well as interpreted fits made using the

PmagPy software package (Tauxe et al., 2016), are available in the MagIC database (https://earthref.org/MagIC/doi/).

Geochronology

Tuffs collected for U-Pb geochronology typically appear as ∼1–5 cm horizons within the Xiajiang Group of the Fanjingshan region. Their tan/white color is distinguishable from the purple/red/green/grey-blue of the adjacent siltstone and fine sandstone. In some cases, the exposed surface of the tuffs have weathered into a clay-rich unlithified mud, likely due to the weathering of the volcanic ash to clays (e.g. bentonite). In these cases, the mud was removed before sampling of the lithified tuff. All samples were scrubbed with steel brushes to remove any recent detritus prior to further analysis.

Standard mineral separation techniques were used to separate zircon grains from bulk rock samples. U-Pb zircon geochronology methods used in this study follow the protocols and data reduction methods of Meyers et al. (2012). Zircon grains were first subjected to chemical abrasion in order to minimize the effects of Pb loss through the removal of zones with radiation damage (Mattinson, 2005). The overall accuracy of the $^{238}U/^{206}Pb$ dates is associated with the gravimetric calibration of the EARTHTIME U-Pb tracer used during the analysis as well as uncertainty associated with the ^{238}U decay constant (Jaffey et al., 1971; Condon et al., 2015). Unless stated otherwise, uncertainties on U-Pb dates reported in this manuscript are the internal (analytical) uncertainties in the absence of external or systematic errors, with these additional uncertainties reported in Table 2.

RESULTS

Paleomagnetism

Thermal demagnetization data from siltstones of the Xiajiang Group in the Fanjingshan region show variable behaviour from site to site. A component removed during initial thermal demagnetization steps (<300°C) is present in most samples and typically yields a direction that is consistent with a present local field overprint acquired via viscous remanent magnetization (Fig. 3). Samples within 29 of the 44 sites yield either unstable or inconsistent behaviour at temperatures >300°C. However, the remaining 15 sites yield stable and consistent behaviour at high temperatures. This high-temperature component is well-fit by least-squares lines that intersect the origin on a Zijderveld plot between ∼650 and ∼690°C (Fig. 3). These high unblocking temperatures are close to the Néel temperature of >500 nm hematite, and are therefore consistent with the high-temperature component being dominantly held by primary detrital hematite rather than finer-grained authigenic pigmentary hematite (Dunlop and Özdemir, 2001; Jiang et al., 2015; Swanson-Hysell et al., 2019).

Two polarities are recorded by the high-temperature component. Of the 15 successful sites, 4 sites yield normal polarity (positive inclination) directions, while the other 11 sites yield reversed polarity (negative inclination) directions (Figs. 2 and 5; Table 1). We interpret positive inclinations to correspond to normal geomagnetic polarity, although we recognize that a correlation of positive inclination to reversed geomagnetic polarity could be permissible in alternative paleogeographic reconstructions. When all sites are converted into a single polarity, the null hypothesis that the specimen mean directions of the normal and reversed polarity sites were drawn from distributions that share a common mean direction can not be rejected at the 95% confidence level (in the Watson V test, $V = 4.9$ and $V_{crit} = 7.4$). Since $V < V_{crit}$, the two polarities recorded by the high-temperature component pass a reversal test after tilt corrections are applied to the high-temperature component site mean directions.

A bootstrap fold test (Tauxe and Watson, 1994) finds that the tightest grouping of site mean directions is obtained between 68 and 103% unfolding at the 95% confidence level (Fig. S1). Since this range of unfolding encompasses 100%, the high temperature component passes a fold test, thereby constraining the high-temperature component to have been acquired prior to Mesozoic folding of the Xiajiang Group (Li et al., 2016a; Ma et al., 2019).

Anisotropy of magnetic susceptibility (AMS) experiments indicate that rocks of the Xiajiang Group have a composite fabric with contributions from an original sedimentary fabric and a weakly developed deformation fabric (Fig. S2; Parés et al., 1999). This fabric is manifest in a grouping of K_{min} axes normal to the deposition plane and a grouping of K_{max} axes as is very typical where fine-grained siliciclastic rocks have experienced any tectonic strain leading to alignment of phyllosilicates (Type II fabric of ParÃ©s, 2015). This weak deformation fabric is consistent with the regional fabric of South China with remanence components in other Tonian/Cryogenian rocks in Guizhou and the surrounding regions having been shown to vary independently of the regional fabric (e.g. Zhang et al., 2013). Additionally, there is no observed correlation between the remanence components of the Xiajiang Group samples and the AMS principle axes.Together, these observations suggest that the high-temperature component of the Xiajiang Group is unaffected by the weak deformation fabric.

Based on the high unblocking temperatures characteristic of detrital hematite, the positive reversal test, and the positive fold test, we interpret the high temperature component (Fig. 5) as being primary and acquired at the time of deposition.

Deposition and burial compaction can result in detrital hematite magnetization being shallower in inclination than the local magnetic field direction at the time of deposition (Tauxe, 2005; Bilardello, 2016). The degree to which the inclination (I) has been shallowed can be expressed by the flattening factor (f) in the equation $\tan(I_{observed}) = f \tan(I_{original})$, where $f = 1$ indicates no inclination shallowing and $f = 0$ indicates a completely flattened direction (King, 1955). Although the flattening factor in any given sedimentary unit depends on a variety of

factors such as the composition of the sediment, values of f obtained from empirical studies of detrital hematite-bearing rocks can be reasonably well-explained by a normal distribution about a mean of ∼0.6 (Tauxe and Kent, 1984; Bilardello, 2016). We therefore apply this empirically-derived inclination correction ($f = 0.6$) to the specimen means obtained from individual sites (Fig. 5), and interpret the resulting direction as approximating the direction of the geomagnetic field at the time of deposition. Directions and poles calculated with and without this inclination correction are shown in Figures 5 and 7.

Geochronology

U-Pb zircon secondary ion mass spectrometry (SIMS) and laser ablation inductively coupled plasma mass spectrometry (LA-ICP-MS) analyses can be conducted relatively rapidly and are often utilized to determine the age of tuff samples. However, U-Pb determinations using SIMS are significantly less precise than those developed with CA-ID-TIMS and are subject to an U-Pb calibration correction that contributes additional uncertainty. This single data point imprecision makes it difficult to recognize real age variation within a sampled population (due to either analyses of domains with Pb loss and/or older zircon). As a result, isotope ratios measured using SIMS can be affected by Pb loss that cannot be identified at the precision of SIMS, which can bias SIMS-derived weighted mean dates toward younger ages. Conversely, deriving a weighted mean from a non-single age population (with variation not resolvable by the single data point analyses) can bias the interpreted age towards being too old. An additional issue in the interpretation of microbeam U-Pb geochronology is that there are dates in the literature where the youngest dates are deconvolved from a larger age population to derive a weighted mean that approximates the ages of eruption. Calculating a weighted mean from the 'young tail' for a distribution of imprecise dates could result in a date that is too young either due to Pb loss in these grains or simply through arbitrary grouping of the youngest dates in a low precision normal distribution of dates. Such a bias could explain calculated SIMS dates from pre-Sturtian strata

313 that are younger than ca. 717 Ma in South China (e.g. Lan et al., 2015) and in practice requires
314 other independent information to defend the interpretation. In addition to the issues surrounding
315 age interpretations, microbeam U-Pb dates require consideration of the U/Pb calibration
316 uncertainty that is typically 1–2% and is a limiting uncertainty.

317 The chemical abrasion step of the CA-ID-TIMS method has been developed to effectively
318 remove (i.e. leach) the analyses of radiation-damaged zones of zircon grains, which are most likely
319 to suffer Pb loss, prior to analysis (Mattinson, 2005). This technique is not perfect – depending
320 on the nature of the material being analysed (U content, zonation patterns), for some samples a
321 proportion of analyses suffering Pb-loss may still persist. The higher-precision of the
322 CA-ID-TIMS single data points often reveals age complexity with excess variance ascribed to
323 geological age variation and residual Pb-loss.

324 Evaluating a hypothesis such as the Bitter Springs Stage TPW hypothesis requires precise age
325 constraints on poles. The SIMS dates prevalent in the literature could have true age uncertainty
326 well beyond the weighted mean uncertainty, particularly if the assumptions made are incorrect
327 (i.e. a single age population, no Pb-loss). As a result, it is essential to develop CA-ID-TIMS dates
328 in order to have high-precision age constraints on paleomagnetic poles.

329 We developed U-Pb CA-ID-TIMS ages from zircon for six tuff samples collected from the
330 Xiajiang Group in the Fanjingshan region (Figs. 2 and 4; Table 2). For each of these ash layers,
331 we make a subjective age interpretation based upon the U-Pb zircon data combined with
332 information about the general nature of the materials. Five tuffs from the lower and middle
333 Xiajiang Group yield dates ca. 816–810 Ma, and one tuff from near the top of the Xiajiang Group
334 in the Hongzixi section yields a younger date of ca. 805 Ma. Within ∼100 m of this youngest tuff,
335 a major unconformity separates ca. 805 Ma sediments of the Xiajiang Group with <717 Ma
336 Sturtian Snowball Earth glacial deposits (Bowring et al., 2007; Macdonald et al., 2010;
337 MacLennan et al., 2018; Lan et al., 2020).

338 Prior to this study, age constraints on Tonian paleomagnetic poles from the Madiyi and

Liantuo formations were based on U-Pb SIMS analyses. In order to improve the precision of these age constraints, as well as evaluate whether they might be biased toward younger ages, we developed new age constraints for these poles using U-Pb CA-ID-TIMS. These new CA-ID-TIMS age constraints supersede the previous SIMS age constraints.

The tuff associated with the paleomagnetic pole for the Madiyi Formation in the Hunan province (sample ZJ-B of Xian et al., 2020) is within the 12 m thick succession of the Madiyi Formation from which the paleomagnetic data were developed. A U-Pb zircon SIMS date of 801.9±6.3 Ma was reported for the tuff in Xian et al. (2020). The new CA-ID-TIMS data from five zircons result in a weighted mean $^{206}Pb/^{238}U$ date of 804.90±0.36 Ma (Fig. 4); Table 2). This date overlaps with the SIMS date of Xian et al. (2020) within uncertainty and constrains the timing of the Madiyi Formation pole to higher precision.

The tuff associated with the paleomagnetic pole for the Liantuo Formation (Evans et al., 2000; Jing et al., 2015) lies ∼15 m below the base of the stratigraphic interval which was sampled for paleomagnetic analysis in Evans et al. (2000) (the upper Liantuo Formation), is approximately stratigraphically equivalent to the stratigraphic interval which was sampled for paleomagnetic analysis in Jing et al. (2021) (the lower Liantuo Formation), and is in the vicinity of a tuff that was previously dated at 748±12 Ma using SIMS (Fig. S6; Ma et al., 1984). The new CA-ID-TIMS data from eight zircons result in a weighted mean $^{206}Pb/^{238}U$ date of 779.52±0.26 Ma – ∼20 m.y. older than the maximum reported uncertainty of the SIMS-derived date (Fig. 4; Table 2).

DISCUSSION

Tectonic Setting

The South China craton consists of two distinct tectonic blocks, the Yangtze and Cathaysia blocks, separated by the Jiangnan Orogen (Fig. 1). However, the depositional setting of sedimentary units in the Jiangnan Orogen as well as the tectonic context of the intrusive units

and deformation found throughout the orogen continues to be debated in the literature. A widely-adopted model proposed that the Fanjingshan Group (and equivalent strata) was deposited in a Grenvillian (ca. 1.3–0.9 Ga) arc-related basin on the Yangtze block as the oceanic crust formerly separating the Yangtze and Cathaysia blocks subducted under the Yangtze block (e.g. Li et al., 2002, 2009). In this model, deformation of the Fanjingshan Group was interpreted to reflect collision of the Yangtze and Cathaysia blocks as the supercontinent Rodinia came together around South China ca. 1.0–0.9 Ga, with Laurentia on the Cathaysia-side of South China and Australia on the Yangtze-side (i.e. the Missing Link model, as shown in Figure 9; Li et al., 1995). The model then proposes that later Tonian (ca. 850–750 Ma) magmatism in the Jiangnan Orogen is associated with a mantle superplume that initiated the break up of Rodinia (e.g. Li et al., 2003, 2009). In this scenario, the Xiajiang Group (and equivalent strata) is interpreted to have been deposited within a failed intra-continental rift basin between the Yangtze and Cathaysia blocks as Australia, South China, and Laurentia rifted apart. Geochronologic and geochemical data initially appeared to support this Missing Link model (e.g. Li et al., 2002, 2003, 2009), and consequently many Neoproterozoic paleogeographic models adopted it (e.g. Li et al., 2008).

However, subsequent geochronologic, geochemical, and paleomagnetic data introduce new constraints that are difficult to reconcile with this model. The timing of Yangtze and Cathaysia block collision represented by the Jiangnan Orogen can no longer be considered to be coeval with the ca. 1080 to 980 Ma Grenvillian Orogen. U-Pb LA-ICP-MS geochronologic constraints from the tuffs, sedimentary rocks, and sills of the Fanjingshan Group (Zhao et al., 2011; Wang et al., 2012; Gao et al., 2014) indicate that deformation of the group occurred after ca. 830 Ma. Our new U-Pb CA-ID-TIMS results constrain initiation of Xiajiang Group deposition, and therefore termination of Fanjingshan Group deformation, to have occurred by 815.73±0.18 Ma (Fig. 2). The interpretation that the Jiangnan Orogeny, and the associated deformation of the Fanjingshan Group, was the result of collision between the Yangtze and Cathaysia blocks gains support from the geochemistry and geochronology of the igneous rocks of the Jiangnan Orogen that are indicative of a supra-subduction, volcanic arc setting (Cawood et al., 2013, 2017).

The Fanjingshan Group is dominated by siliciclastic sediments and also contains horizons of volcanic rocks including pillow basalts (Zhou et al., 2009). These units were intruded by ca. 830 Ma mafic sills with geochemical signatures consistent with subduction-related magmatism (Wang et al., 2014) as well as 835±5 Ma (U-Pb SIMS) felsic intrusive rocks (Fig. 1B; Gao et al., 2011). Both fore-arc (Zhao et al., 2011) and retro/back-arc (Lin et al., 2016; Yao et al., 2019) settings have been interpreted for the Fanjingshan Group deposition. However, fore-arc settings are typically cold and amagmatic, and consequently we prefer a syn-collisional retro-arc foreland model with ultramafic magmatism associated with slab-breakoff. In either model, the Fanjingshan Group was deposited and intruded in an arc-related basin as the oceanic crust formerly separating the Yangtze and Cathaysia blocks subducted under the Yangtze block (Lin et al., 2016). As Yangtze and Cathaysia (or at least a portion of Cathaysia) collided between ca. 830 Ma and 815.73±0.18 Ma, sedimentary rocks of the Fanjingshan Group were folded, uplifted, and eroded. Following this deformation and the development of an erosional unconformity, subsidence enabled deposition of the overlying Xiajiang Group. Taken together, these data constrain the collision of the Yangtze and Cathaysia blocks to have occurred between ca. 830 Ma and 815.73±0.18 Ma, not ca. 1000 to 900 Ma as is proposed in the Missing Link model implemented in Li et al. (2008).

In addition to this evidence of Tonian convergence between the Yangtze and Cathaysia blocks, the record of the northwest Yangtze block indicates a convergent tectonic setting in the Tonian that extended into the Cryogenian. Geochronologic and geochemical constraints from the Panxi-Hannan Belt (Fig. 1) indicate that arc-related magmatism was occurring in that belt ca. 870–706 Ma (Dong et al., 2012), and therefore that the northwestern margin of the Yangtze block was an active margin throughout the time that Rodinia is hypothesized to have been a coherent supercontinent. This arc-related magmatic activity associated with subduction along the northwestern margin of the Yangtze block is the likely source for the ashes that formed the tuffs within the Xiajiang Group that we have targeted for geochronology (Fig. 2).

Finally, paleomagnetic constraints indicate that South China was at high latitudes throughout

the late Tonian (discussed further in *Tonian APWP of South China*) rather than at low-latitudes as would be required by the Missing Link model (discussed further in *South China and Rodinia*; Fig. 9). Additionally, the paleomagnetic data suggests that the Panxi-Hannan Belt lay from the east to the north relative to the Fanjingshan region in reconstructed coordinates during the time of Xiajiang Group deposition (ca. 815–800 Ma; Fig. 7). At these high latitudes, the prevailing winds are polar easterlies, which is consistent with the idea that the ashes that formed the tuffs within the Xiajiang Group were transported from the Panxi-Hannan Belt (Hildebrand, 1988).

Together, these constraints are inconsistent with South China being within the interior of a stable supercontinent during the Tonian. Instead, they indicate a convergent setting with the northwestern margin of the Yangtze block being an active margin into the Cryogenian rather than being juxtaposed against a conjugate continent. Therefore, the data are more compatible with South China on the periphery of Rodinia or disconnected from it entirely (Fig. 9).

The tectonic setting of the basin in which the Xiajiang Group (and equivalent strata) was deposited is commonly interpreted as a failed intra-continental rift basin (Zhang et al., 2019), potentially associated with the hypothesized mantle superplume that initiated the break up of Rodinia (Li et al., 2003, 2009). However, this basin development framework is rooted in a tectonic setting interpretation that would have South China within the interior of a supercontinent undergoing break-up — a setting that is inconsistent with available constraints. Rather, any basin development model needs to honor the following:

- There was a geologically short interval (ca. 15 m.y.) between the orogenesis that deformed the Fanjingshan Group and the subsidence that enabled deposition of the Xiajiang Group.
- There was an active margin along the northwestern margin of the Yangtze block at the time of Xiajiang Group subsidence. This margin is the likely source of the tuffs throughout the Xiajiang Group stratigraphy.
- The site of Xiajiang Group deposition must have been folded, uplifted, and eroded prior to

441 subsidence.

442 • Subsidence rates were initially quite high as evidenced by the rapid sediment accumulation
443 rates in the Xiajiang Group. These high subsidence rates led to the deep-water setting of
444 the Xiajiang Group sediments.

445 • While some strata could be missing through glacial erosion, the duration of missing time
446 (∼90 m.y.) in the ca. 805 and 717 Ma pre-Sturtian unconformity suggests limited sediment
447 accumulation in the pre-Sturtian interval relative to the thick ca. 815 to 805 Ma succession.

448 The Nanhua Basin into which the Xiajiang Group was deposited formed inland from the
449 Panxi-Hannan Belt (Cawood et al., 2017). Based on the interpretation that the Panxi-Hannan
450 Belt was an active arc at the time of Xiajiang Group deposition, Qi et al. (2019) argued that
451 Nanhua Basin formation was the result of back-arc extension. Importantly, the timing of
452 deposition of the Xiajiang Group coincides with the initiation of back-arc extension in the
453 Panxi-Hannan arc (Dong et al., 2012). Back-arc extension provides a mechanism to explain
454 regional extension and subsidence in the region of the Jiangnan suture. Furthermore, given that
455 back-arc basin formation is the result of the combined driving mechanisms of surface kinematics
456 and dynamic mantle flow (Sdrolias and Müller, 2006), it can lead to both rapid and transient
457 subsidence. Geologic observations in more recent back-arcs have been interpreted to indicate
458 significant back-arc extension in regions where lithosphere has been thickened through orogenesis
459 (Göğüş, 2015). Numerical modeling has shown that post-orogenic lithosphere removal (such as
460 that occurring as a result of delamination) in continental back-arc settings can lead to large-scale
461 subsidence (Göğüş, 2015). This mechanism could explain the transition at the site of Xiajiang
462 Group deposition from folding, uplift, and erosion in the Jiangnan Orogen as Yangtze collided
463 with Cathaysia between ca. 830 Ma and 815.73±0.18 Ma, to Nanhua Basin subsidence as a
464 back-arc basin formed. The Nanhua Basin is therefore best interpreted as a polyphase basin
465 wherein this Tonian subsidence was followed by Cryogenian and Ediacaran subsidence potentially
466 as the result of other mechanisms. The tuffs found throughout the Xiajiang Group stratigraphy

are the result of the arc on the northwestern margin of the Yangtze block that was active throughout deposition, both driving subsidence through back-arc extension and contributing ashes via the prevailing polar easterly winds that enable us to develop geochronologic constraints.

Tonian APWP of South China

With the exception of the highest ash sample in the Hongzixi section, all dated ash samples from the Xiajiang Group of the Fanjingshan region yield ages of ca. 816–810 Ma (Fig. 2). Furthermore, the high temperature components in all sites record similar directions (Fig. 5). We therefore take the parsimonious interpretation that variability in the high temperature component between specimens/sites is largely recording short time-scale secular variation in the magnetic field, and therefore develop a single paleomagnetic pole from the mean direction of the high temperature component from all sites (Fig. 5). Based on the geochronologic constraints (Fig. 2), we assign a nominal age to this pole of 813±3 Ma. However, we discuss the possibility of multiple poles being recorded in the Xiajiang Group below.

This new pole can be combined with existing Neoproterozoic paleomagnetic poles for South China (summarized in Table 3) to develop an apparent polar wander path (APWP). There are complications associated with the interpretation of some of these poles and their assigned ages and we will discuss each in turn.

The Yanbian dikes pole (Niu et al., 2016) was obtained from a deformed region on the western-most margin of the South China craton that experienced vertical axis rotation during the Cenozoic collision of India with Asia (Zhu et al., 2008; Zheng et al., 2010; Gao et al., 2017). The magnitude of this vertical axis rotation was estimated to be 5.3±3.0° based on paleomagnetic data from Pliocene sedimentary rocks in the region (Zhu et al., 2008), and Niu et al. (2016) applied a 5° vertical axis rotation correction to their Yanbian dikes pole. However, the vertical axis rotation correction may be as little as 2.3° or as high as 8.3° at the 95% confidence level (Zhu et al., 2008). The Yanbian dikes may also have experienced pre-Pliocene vertical axis rotation.

Furthermore, no tilt-correction was applied to the majority of the directions obtained from the Yanbian dikes, despite observations that the dikes exhibit dips that range from 43° to vertical (Niu et al., 2016). Finally, the Yanbian dikes pole is inconsistent with the Xiaofeng dikes pole (Fig. 7A) despite the similar age of these two poles. Given these complications, we exclude the Yanbian dikes pole as a constraint in our preferred Tonian South China APWP (Fig. 7C).

The Xiaofeng dikes pole has had both its direction and age revised since its initial publication in Li et al. (2004). Jing et al. (2020) argued that a subset of the dikes that were used to obtain the Xiaofeng dikes pole are located between two faults and have paleomagnetic directions that may have been rotated relative to the rest of the dikes. Therefore, to account for the possibility of vertical axis rotation affecting this subset of dikes, Jing et al. (2020) recalculated the Xiaofeng dikes pole by excluding them. The resulting pole is closer to the other ca. 820-800 Ma poles for South China (Fig. 7), although further work is needed to substantiate whether this difference in pole position is robust, especially since it has been argued that the entire central Yangtze region experienced some vertical axis rotation (Shen et al., 1999). In addition, the Xiaofeng dikes were originally dated to 802±10 Ma based on U-Pb SIMS analyses on zircon from the dikes (Li et al., 2004). When zircon from these dikes were reanalyzed at higher precision using CA-ID-TIMS, their age was revealed to be significantly older (821.64±0.2 Ma; Wang et al., 2016b). This revised age constraint for the Xiaofeng dikes pole is utilized here (Table 3; Fig. 7).

The previous age constraint on the Madiyi Formation pole of 801.9±6.3 Ma was also developed using U-Pb SIMS measurements on zircon from a tuff within the section where the paleomagnetic data were developed (Xian et al., 2020). Our new CA-ID-TIMS date of 804.90±0.36 Ma is within the uncertainty of this SIMS date and provides a higher precision age constraint on the age of the pole (Fig. 4) which supersedes the previous age and is utilized here (Table 3; Fig. 7).

The paleomagnetic pole for the upper Liantuo Formation (Member 2) has long been an important constraint for the Neoproterozoic paleogeography of South China (Evans et al., 2000). The Liantuo Formation unconformably overlies the Huangling granite suite for which U-Pb SIMS

518 dates of 863±9, 844±10, and 842±10 Ma have been developed (Wei et al., 2012). These granites
519 are intruded by the 821.64±0.2 Ma Xiaofeng dikes (Wang et al., 2016b). The Liantuo Formation
520 is unconformably overlain by Cryogenian glacial deposits. The age assigned to the Liantuo
521 Formation pole has varied in the literature. When a paleomagnetic pole from the formation was
522 first reported in Evans et al. (2000), it was assigned an age of 748±12 Ma based on an U-Pb
523 SIMS date on a tuff ∼15 m below the base of the stratigraphic interval that was sampled for
524 paleomagnetic analysis (Ma et al., 1984; Fig. S6). When this paleomagnetic pole was updated in
525 Jing et al. (2015) with the addition of paleomagnetic data from additional sites to the southwest
526 of the stratigraphic section sampled in Evans et al. (2000), its age was interpreted to be ca.
527 720 Ma based on U-Pb SIMS dates on tuffs within the upper 20 m of the Liantuo Formation
528 across the Three Gorges Area (Lan et al., 2015). A challenge with these U-Pb SIMS dates is that
529 there is a distribution of dated grains around a peak of ca. 780 to 770 Ma that includes sparse
530 younger dates (Fig. 4; Lan et al., 2015). In Lan et al. (2015), these younger dates are interpreted
531 as the eruptive age of the tuffs, but it is possible that these grains are biased young. Ambiguity
532 associated with correlation of the Liantuo Formation with possibly equivalent stratigraphy adds
533 further complexity to the interpretation of geochronologic constraints on the Liantuo Formation.
534 For example, zircons from a tuffaceous siltstone ∼25 m below Sturtian glacial deposits in the
535 Gongdong Formation of northern Guangxi, which is often interpreted to be a deeper water
536 equivalent to the Liantuo Formation (Wang and Li, 2003; Pi and Jiang, 2016), yield a weighted
537 mean CA-ID-IRMS date of 720.16±1.40 Ma (Lan et al., 2020). If this interpretation that the
538 Gongdong Formation correlates to the Liantuo Formation is correct, it suggests that, at least in
539 some parts of the Nanhua Basin, sediments as young as ca. 720 Ma are preserved. On the other
540 hand, if the two formations are not correlative, then the CA-ID-IRMS date of 720.16±1.40 Ma
541 (Lan et al., 2020) does not place any geochronologic constraints on the Liantuo Formation.
542 Finally, an additional pole for the lower Liantuo Formation (Member 1) was reported in Jing
543 et al. (2021), based on paleomagnetic data from sites to the west of the stratigraphic sections
544 sampled in Jing et al. (2015). The lower Liantuo Formation pole lies slightly closer to the other

ca. 800 Ma poles for South China than the upper Liantuo Formation pole (Fig. 7).

We have developed a new CA-ID-TIMS date of 779.52±0.26 Ma for a tuff in the Liantuo Formation at the same location studied by Ma et al. (1984). Similar to the updated Xiaofeng dikes geochronology, this date is appreciably older than interpretations based on the previous SIMS U-Pb dates. It is possible that some or all of the zircons included in the calculation of the weighted mean date may be detrital and not representative of the eruptive age of the tuff, but the consistency of the zircon dates (Fig. 4) suggests that the weighted mean date represents an eruptive age. Stratigraphically, this tuff correlates with the paleomagnetic sites in the lower Liantuo Formation sampled in Jing et al. (2021) (Fig. S6), hence we pair this new age constraint with this paleomagnetic pole for the lower Liantuo Formation. However, this tuff also provides a high-precision geochronologic constraint for the upper Liantuo Formation. The tuff lies ∼15 m below the stratigraphic interval sampled by Evans et al. (2000), and the the similar lithologies throughout this interval (fine to medium sandstone interbedded with siltstone; Fig. S6) suggests conformable deposition. Therefore, the age of the tuff is unlikely to be tens of millions of years older than the sedimentary rocks from which the paleomagnetic data for the upper Liantuo Formation were developed. As such, we prefer the interpretation that the age of the upper Liantuo Formation and its pole is close to 779.52±0.26 Ma and that the Liantuo Formation is not correlative to the ca. 720 Ma Gongdong Formation, although without further high-precision geochronologic constraints from higher in the Liantuo Formation stratigraphy the possibility remains that the upper Liantuo Formation pole post-dates this date.

The existing date of 799.5±8.4 Ma for the Chengjiang Formation pole was also developed using SIMS (Table 3). As evidenced for the Xiaofeng dikes and the Liantuo Formation, when SIMS-derived ages are re-investigated through CA-ID-TIMS, the result can be a significantly different date. Therefore, the accuracy of the SIMS-derived dates for the Chengjiang Formation pole remains uncertain.

The Xiajiang Group paleomagnetic pole developed in this study is calculated as a site mean

(i.e. the mean of the means of specimen directions for each site; Fig. 5). However, the Madiyi Formation pole is reported in Xian et al. (2020) as a specimen mean (i.e. the mean of specimen directions across all sites). While both methods can be justified for sedimentary rocks, the specimen mean direction leads to paleomagnetic poles with smaller A_{95} uncertainty ellipses due to the larger number of directions used to obtain the mean which has the potential to underestimate the uncertainty. We recalculate the paleomagnetic poles for the Madiyi Formation as a site mean, to be consistent with the methodology used to develop our Xiajiang Group pole (Fig. 7).

An inclination correction has been applied to the paleomagnetic pole obtained from the Xiajiang Group in this study. Similarly, an inclination correction was applied to the pole obtained from the Madiyi Formation (Xian et al., 2020). Given that the poles from the Chengjiang and Liantuo formations are also derived from the hematite-held magnetization of similar siliciclastic sedimentary rocks, we apply the same inclination correction ($f = 0.6$) to these poles as that applied to the Xiajiang Group and Madiyi Formation poles (Fig. 7). Given potential variability in inclination shallowing, the flattening could vary from this value which is an additional source of uncertainty.

The 821.6±0.2 Ma Xiaofeng dikes and the inclination-corrected 804.9±0.4 Ma Madiyi and 799.5±8.4 Ma Chengjiang poles all overlap within uncertainty, and the ca. 816-810 Ma Xiajiang Group records a distinct, but similar, position as well (Fig. 7). Together, these poles constrain South China to have been in a roughly stable position at high latitudes ($\gtrsim$60°) ca. 820–800 Ma (Figs. 7 and 8). The ∼779.5±0.3 Ma and <779.5±0.3 Ma Liantuo Formation poles also constrain South China to be at high latitudes, although with a different orientation to the ca. 820–800 Ma position (Figs. 7 and 8). The poles constrain South China to be at high latitudes in the latter half of the Tonian, likely drifting across the pole after ca. 805 Ma (Fig. 7).

South China and Rodinia

Connections between Siberia (Ernst et al., 2016; Evans et al., 2016), Australia-East Antarctica (Veevers and Eittreim, 1988; Duebendorfer, 2002; Goodge et al., 2008; Goodge and Fanning, 2010; Li and Evans, 2011; Swanson-Hysell et al., 2012; Eyster et al., 2019), and the western margin of Laurentia are reasonably well-established for the late Tonian (Fig. 9). Paleomagnetic poles from India ca. 1070 and 750 Ma permit a connection with northwest Australia through the Tonian (Swanson-Hysell et al., 2012), although it has also been suggested that India was disconnected from Rodinia during this time (Merdith et al., 2017). Within this paleogeographic context of northern Rodinia, three models of South China's relationship with Rodinia have been proposed, which we refer to as the "Missing Link," "Periphery," and "Separate" models (Fig. 9).

The Missing Link model proposes that the supercontinent Rodinia came together around South China ca. 1.0–0.9 Ga, with Laurentia on the Cathaysia-side of South China and Australia on the Yangtze-side (Fig. 9).Paleomagnetic poles from South China including the new Xiajiang Group pole constrain it to be at high latitudes from ca. 821 Ma to at least 780 Ma (*Tonian APWP of South China*, Fig. 7), whereas paleomagnetic data from Australia, Laurentia, and Siberia constrain those cratons to be at relatively low latitudes ca. 775 Ma (Figs. 8 and 9). The collision between the Yangtze and Cathaysia blocks between ca. 830 Ma and 815.73±0.18 Ma and subduction along northwestern Yangtze ca. 870-706 Ma also cannot be reconciled with a position of South China within the interior of a stable supercontinent anytime in the Tonian Period.

On the other hand, the Periphery model (Fig. 9) is consistent with both the paleomagnetic constraints as well as our current understanding of the tectonic context of South China. In our Periphery model configuration, South China is at high latitudes, connected to Rodinia via northwestern India. Yangtze is free to have travelled across an open ocean to collide with Cathaysia between ca. 830 Ma and 815.73±0.18 Ma. Northwestern Yangtze faces this open ocean, allowing for subduction along that margin in the Tonian and into the Cryogenian. Tonian volcanism in northwest India shares geochemical characteristics with arc magmatism in the

Panxi-Hannan Belt (Ashwal et al., 2013; Cawood et al., 2017), which has been interpreted as the result of a continuous subduction zone along northwestern Yangtze and western India and consistent with a connection between western South China and northwestern India. Detrital zircon spectra of Cryogenian sediments in South China also appear similar to that observed in northwestern India, further supporting this connection (Cawood et al., 2017; Qi et al., 2020). However, the ca. 755 Ma paleomagnetic poles result in a Periphery model configuration that differs from the paleogeographic models proposed in the literature that also place South China along the periphery of Rodinia (Fig. 9). For example, it has been proposed that India-South China was connected to Rodinia, but further south along the western margin of Rodinia such that eastern India was juxtaposed against western East Antarctica and eastern South China was juxtaposed against western Australia (Cawood et al., 2017). However, ca. 755 Ma paleomagnetic poles from South China, India, and Australia are inconsistent with this alternative position.

It has also been proposed that India-South China was disconnected from Rodinia entirely (Merdith et al., 2017). In this Separate model, the Rayner province is also interpreted to be a terrane disconnected from Rodinia that amalgamated with India ca. 900 Ma resulting in the Eastern Ghats Orogen in eastern India, with subduction continuing along Rayner's margin until India-Rayner collides with East Antarctica near the Precambrian-Cambrian boundary (Merdith et al., 2017). In contrast, other models of Rodinia interpret Rayner to have been part of Rodinia by 900 Ma, and that the Eastern Ghats Orogen records amalgamation of India with Rodinia (Li et al., 2008). Current geologic constraints from Rayner do not differentiate between these two scenarios.

Importantly, paleomagnetic data indicate that South China drifted across the pole after ca. 800 Ma (Fig. 7). In order to satisfy these paleomagnetic constraints, the Periphery model in which South China is in a constant position relative to the core of Rodinia would need to call upon anticlockwise vertical axis rotation of the entire Rodinia supercontinent(Fig. 9). Furthermore, the Periphery model would imply that the Lower and Upper Grusdievbreen

Formation poles from Svalbard are inconsistent with the paleomagnetic data from South China, and therefore require that the Svalbard poles cannot be interpreted as robust ca. 800 Ma paleomagnetic constraints on the configuration and orientation of Rodinia. On the other hand, the Separate model does not require rotation of Rodinia to satisfy the paleomagnetic constraints from South China, and could allow the Svalbard poles to be reconciled with the South China poles.

A fourth model of South China's relationship with Rodinia has also been proposed (the "Inverted South China" model), which places India-South China in the southern hemisphere connected to Rodinia via Kalahari until ca. 780 Ma (Jing et al., 2021). The model then hypothesizes that India-South China moves rapidly northward toward a position close to Australia (such as that depicted in the Separate model of Figure 9) via a large dextral strike-slip fault ca. 780-760 Ma. The new paleomagnetic data in (Jing et al., 2021) are from the lower Liantuo Formation and are similar to previous poles from that formation, albeit implying a slightly higher latitude position than poles from the upper Liantuo Formation, consistent with a progressive APWP path (Fig. 7). However, rather than being based on these Liantuo Formation poles, the interpreted position of India-South China in the southern hemisphere before ca. 780 Ma is based on inverting the polarity of older South China poles and seeking to satisfy a subset of poles from the Yanbian dikes (Group B) and a subset of poles from the Chengjiang Formation sites (CJH3; Jing et al., 2021). However, the Yanbian dikes Group B pole used in this reconstruction is comprised of just 3 dikes (Niu et al., 2016), and, as discussed above, may have experienced vertical axis rotation. Furthermore, the CJH3 directional grouping from the Chengjiang Formation sites does not have a supporting field test and is from a section that lacks geochronologic constraints (the Douzui Village section in Jing et al., 2020). Given the ambiguity regarding these poles, these constraints should not be prioritized in the reconstruction of South China in the Tonian and we exclude them from our paleogeographic models.

Bitter Springs Stage True Polar Wander

TPW should result in the same magnitude of angular change in paleomagnetic pole positions for all continents. As a result, the Bitter Springs Stage TPW hypothesis predicts a ∼50° change in pole position between pre-Bitter Springs Stage poles (>ca. 810 Ma) and syn-Bitter Springs Stage poles (ca. 810 to 795 Ma), with a similar angular difference between syn-Bitter Springs Stage poles and post-Bitter Springs Stage poles (<ca. 795 Ma).

Paleomagnetic data from the Xiajiang Group of the Fanjingshan region have the potential to test this hypothesis. Our U-Pb dates demonstrate that there are Xiajiang Group sedimentary rocks that are both older and younger than the onset of the Bitter Springs Stage (ca. 810 Ma) preserved in at least some parts of the Fanjingshan region (Fig. 2). The bulk of the high temperature component paleomagnetic data (11 of 15 sites) were developed from strata below tuffs that are dated to be >810 Ma, and are therefore constrained to have been deposited prior to the Bitter Springs Stage. However, the remaining 4 sites could have been deposited during the Bitter Springs Stage. One site that yielded a stable and consistent high temperature component in the Hongzixi section is bracketed by tuffs that constrain it to be between 809.52±0.50 Ma and 804.56±0.39 Ma (Fig. 2). However, this site cannot definitively be interpreted to have been deposited during the Bitter Springs Stage, since the onset of the Bitter Springs Stage can only be constrained to have occurred after 811.51±0.25 Ma (based on CA-ID-TIMS on a tuff ∼50 m below carbonates that record the first abrupt shift to negative δ^{13}C values in the Fifteenmile Group of northwest Canada; Macdonald et al., 2010) and before ca. 807.9±0.2 Ma (based on interpolation between geochronologic constraints paired to the δ^{13}C record; Swanson-Hysell et al., 2015). Paleomagnetic data were not developed from sediments in the Hongzixi section in the proximity of the tuff that yielded the 804.56±0.39 Ma date, because these coarser-grained sediments were judged in the field to be not as amenable for preserving a primary magnetic remanence and were not sampled. Another site in the Kuaichang section is above a tuff dated at 811.47±0.67 Ma (Fig. 2). However, the age of this site may be very close to 811.47±0.67 Ma, and therefore also cannot

be unambiguously interpreted to have been deposited during the Bitter Springs Stage. Stable dual-polarity paleomagnetic data were developed from the uppermost Xiajiang Group at two sites in the Mamagou section ∼35 m below the unconformity with the overlying Cryogenian glacial sediments (Fig. 2). If this unconformity is assumed to be time-correlative between the Hongzixi and Mamagou sections, then these Mamagou sites approximately correlate to the 804.56±0.39 Ma tuff in the Hongzixi section, suggesting that they are syn-Bitter Springs Stage in age. However, the Mamagou section lies ∼20 km to the south of the Hongzixi section, and along-strike variability of the erosional unconformity at the top of the Xiajiang Group could have resulted in the Mamagou section not being syn-Bitter Springs Stage in age.

We compare the high temperature components obtained from the 11 sites that are unambiguously pre-Bitter Springs Stage, with the high temperature components obtained from the four sites that could be syn-Bitter Springs Stage. After converting all sites into a single polarity and applying a tilt and inclination correction, the two site mean directions have an angular difference of 3.0°, and a common mean test cannot reject the null hypothesis at the 95% confidence level that the specimen mean directions were drawn from distributions that share a common mean direction (in the Watson V test, $V = 0.8$ and $V_{crit} = 6.9$; Fig. 6). This angular difference is much less than would be expected for Bitter Springs Stage TPW, indicating that the Nanhua Basin was in a similar position throughout Xiajiang Group deposition and that the sites can be grouped into a single paleomagnetic pole. However, ambiguity surrounding the age of the 4 sites that could be syn-Bitter Springs Stage hinders the ability to draw firm conclusions regarding TPW using the Xiajiang Group data alone. To gain more robust insight, we can assess the Xiajiang Group data in the context of the other Tonian South China poles.

The new 813±3 Ma Xiajiang Group pole and the new 804.9±0.4 Ma date on the Madiyi Formation pole provide paleomagnetic constraints on the position of South China before and during the Bitter Springs Stage. Additionally, the 821.6±0.2 Ma date on the Xiaofeng dikes pole constrains it to be pre-Bitter Springs Stage (although prior interpretations have taken the

722 Xiaofeng dikes pole to represent a syn-Bitter Springs Stage position of South China using its
723 previously assigned age of 802±10 Ma; Maloof et al., 2006; Jing et al., 2020). The pre-Bitter
724 Springs Stage Xiaofeng dikes pole and the syn-Bitter Springs Stage Madiyi Formation pole share
725 a common mean (Fig. 7). Interpreting these two poles alone would suggest that South China was
726 in a stable position between ca. 821 and 805 Ma inconsistent with the prediction of the TPW
727 hypothesis.

728 However, the pre-Bitter Springs Stage Xiajiang Group pole has a distinct position from the
729 syn-Bitter Springs Stage Madiyi Formation pole, with an angular difference of 19° between the
730 means of the poles (Fig. 7). In order to assess this angular difference in comparison to the poles
731 from Svalbard while accounting for the uncertainty on the pole positions and ages, we take a
732 Monte Carlo approach in which 10,000 random draws are taken from Fisherian distributions for
733 the pole positions and from Gaussian distributions for the pole ages (Figs. 10A and 10B;
734 Swanson-Hysell et al., 2014). Taking this approach, the angular difference between the Xiajiang
735 Group and Madiyi Formation poles is 11–27° at the 95% confidence level, whereas the angular
736 difference between the Lower and Upper Grusdievbreen Formation poles is much higher at 41–62°
737 at the 95% confidence level (Fig. 10C). In fact, the probability that a Xiajiang Group–Madiyi
738 Formation pole pair has an equal or larger angular difference than a Lower–Upper Grusdievbreen
739 Formation pole pair is only 8.5×10^{-5}% (calculated using the means and standard deviations of
740 the normal distributions in Fig. 10C). As such, the angular difference between the pre- and
741 syn-Bitter Springs Stage poles is significantly less than predicted by the hypothesis that the
742 Svalbard paleomagnetic poles are primary and that their differing positions is the result of TPW.
743 Therefore, this Monte Carlo analysis suggests that the angular difference between the pole pairs
744 from South China and Svalbard can not be straight-forwardly interpreted to be associated with a
745 single TPW rotation.

746 The velocity of South China implied by the Xiajiang Group and Madiyi Formation poles is
747 also slower than that implied for Svalbard by the Lower and Upper Grusdievbreen Formation

poles, being 14–48 cm/yr rather than 60–284 cm/yr at the 95% confidence level, if the Upper Grusdievbreen Formation pole is taken to be 1 to 10 m.y. younger than the Lower Grusdievbreen Formation pole (Maloof et al., 2006; Fig. 10D). In contrast to the very rapid rates implied by the Svalbard poles, the rate for South China's motion is at the upper end of the range of velocities suggested by plate kinematic reconstructions (Fig. 10D; Meert et al., 1993; Zahirovic et al., 2015).

However, the smaller angular difference between the Xiajiang Group and Madiyi Formation poles relative to the Lower and Upper Grusdievbreen Formation poles could be reconciled with the TPW hypothesis if differential plate motion between South China and Svalbard is superimposed on TPW motion between ca. 813 and 805 Ma (Evans, 2003). For example, if rapid TPW occurred ca. 810 Ma, the Xiajiang Group and Madiyi Formation poles should lie along the great circle between the Lower and Upper Grusdievbreen Formation poles, implying a unique reconstruction for South China relative to Svalbard (Fig. 11). This configuration also aligns the great circle between the syn-Bitter Springs Stage Upper Grusdievbreen Formation and post-Bitter Springs Stage Svanbergfjellet Formation Svalbard poles with that of the syn-Bitter Springs Stage Madiyi Formation and post-Bitter Springs Stage Liantuo Formation South China poles (Fig. 11). In the TPW hypothesis, this second great circle would represent the second rapid TPW event ca. 795 Ma. However, South China could have continued to move via differential plate tectonics along the trajectory implied by the difference between the ca. 821 Ma Xiaofeng dikes and the ca. 813 Ma Xiajiang Formation poles through ca. 810 Ma TPW rotation (Fig. 11). In such a scenario, the differential plate tectonic motion of South China is approximately opposite the trajectory of the hypothesized TPW rotation (Fig. 11), which would be observed in the paleomagnetic record as a smaller angular difference between pre- to syn-Bitter Springs Stage paleomagnetic poles from South China than what would be predicted for TPW alone. Put another way, differential plate tectonic motion could have driven South China in the opposite direction of TPW motion, causing South China to move a smaller distance in a celestial (spin axis) reference frame relative to other tectonic blocks that were not experiencing such differential plate tectonic motion between ca. 813 and 805 Ma, such as Svalbard.

775 Importantly, if rapid TPW did occur ca. 810 Ma, and differential plate motion between South
776 China and Svalbard ca. 813–805 Ma is superimposed upon that TPW motion to explain the
777 smaller angular difference between the Xiajiang Group and Madiyi Formation poles relative to
778 the Lower and Upper Grusdievbreen Formation poles, then it is required that South China was
779 separate from Rodinia (i.e. the Separate model in Figure 9). It is well established that Svalbard
780 was connected to Laurentia via Greenland until Silurian-Devonian translation along Greenland's
781 margin and subsequent rifting away from Greenland in the Eocene (Torsvik and Cocks, 2016).
782 Therefore, if South China was moving differentially relative to Svalbard ca. 813–805 Ma, South
783 China must have been moving differentially relative to Rodinia, and therefore must have been
784 separate from Rodinia. Furthermore, the alignment of paleomagnetic poles from South China and
785 Svalbard along great circles places South China at high latitudes, with the long southeastern
786 margin of the Cathaysia block facing Svalbard (Fig. 11). However, ca. 755 Ma paleomagnetic
787 poles require that a Periphery model has South China-India-Rayner connected to Rodinia in a
788 different orientation via northwestern Australia (Fig. 9). Even if the Lower Grusdievbreen
789 Formation pole is interpreted as a Paleozoic overprint (Michalski et al., 2011), if the syn-Bitter
790 Springs Stage Upper Grusdievbreen Formation and post-Bitter Springs Stage Svanbergfjellet
791 Formation Svalbard poles are primary, rapid TPW could be interpreted to have occurred ca.
792 795 Ma. In this scenario, South China is still required to be separate from Rodinia in order to
793 align the great circle between path with that of the syn-Bitter Springs Stage Madiyi Formation
794 and post-Bitter Springs Stage Liantuo Formation South China poles (Fig. 11).

795 Regardless of whether the ca. 821 Ma to ca. 805 Ma poles are interpreted as recording TPW
796 counteracted by plate tectonic motion or a relatively stable position of South China in a scenario
797 without TPW (Fig. 12), South China is peripheral and likely disconnected from Rodinia.

CONCLUSIONS

The geochronologic and paleomagnetic data developed from the Xiajiang Group constrain the amalgamation of the Yangtze and Cathaysia blocks of South China to have completed between ca. 830 Ma and 815.73±0.18 Ma at high latitudes. A consistent high latitude position is implied by poles from ca. 821 Ma to 805 Ma with a continued high latitude position ca. 780 Ma following South China transiting over the pole. These paleolatitudes, as well as convergent orogenesis between the Yangtze and Cathaysia blocks and continued arc activity along the northwest margin of the South China craton during the Tonian and into the Cryogenian, cannot be reconciled with the Missing Link model that places South China in the core of a stable Rodinia continent. The angular difference in pole position between the ca. 813 Ma (pre-Bitter Springs Stage) Xiajiang Group pole and ca. 805 Ma (syn-Bitter Springs Stage) Madiyi Formation pole is significantly less than that predicted for the Bitter Springs Stage TPW hypothesis. The poles could be interpreted to indicate a relatively stable high latitude position for South China inconsistent with TPW. However, it is possible to interpret the poles as TPW rotation counteracted by plate tectonic motion. In this scenario, South China must be considered to be distinct from Rodinia. Whether or not the paleomagnetic poles are interpreted as recording TPW, they constrain South China to either have been connected to Rodinia along its periphery, or disconnected from the (super)continent entirely.

ACKNOWLEDGEMENTS

Code and data used in this study is available on Zenodo at https://doi.org/10.5281/zenodo.4660237 and GitHub at https://github.com/Swanson-Hysell-Group/Banxi_Paleomagnetism. The paleomagnetic data have also been uploaded to the MagIC database https://www2.earthref.org/MagIC. Research was supported by National Science Foundation grants EAR-1547434 and EAR-1547537 to N.L.S-.H.

822 and F.A.M. CUGB research was supported by National Natural Science Foundation of China
823 grant 41830215 to S.H.Z. Maoyan Zhu supported research logistics in the field. Oliver Abbitt
824 prepared specimens for paleomagnetic analyses.

TABLES

Table 1. Paleomagnetic results for individual sites with stable and consistent high temperature components in the Xiajiang Group of the Fanjingshan region.

site	section	lab	site lat.	site lon.	n	$\mathbf{dec}_{1.0}$	$\mathbf{inc}_{1.0}$	$\mathbf{dec}_{0.6}$	$\mathbf{inc}_{0.6}$	α_{95}	k	polarity
TR007	Hongzixi	Beijing	27.991	108.797	13	14.1	64.4	14.1	73.9	8.9	22.8	N
TR014	Hongzixi	Berkeley	28.014	108.805	12	150.2	-66.8	330.2	75.6	12.1	14.0	R
TR018	Kuaichang	Berkeley	27.867	108.820	14	208.3	-64.0	28.3	73.7	14.2	9.0	R
TR020	Kuaichang	Berkeley	27.866	108.821	10	111.6	-76.9	291.6	82.1	11.2	20.0	R
TR021	Kuaichang	Beijing	27.864	108.822	9	208.0	-71.5	28.0	78.6	17.0	10.1	R
TR024	Kuaichang	Berkeley	27.872	108.811	9	124.9	-63.5	304.9	73.3	18.2	9.0	R
TR026	Kuaichang	Berkeley	27.872	108.811	9	150.3	-85.7	330.3	87.4	16.0	11.0	R
TR004a	Mamagou	Berkeley	27.835	108.797	10	334.8	71.4	334.8	78.6	8.2	35.3	N
TR004b	Mamagou	Berkeley	27.835	108.797	5	106.4	-75.9	286.4	81.4	12.6	37.9	R
TR031	Luoman	Beijing	27.938	108.831	8	337.6	65.2	337.6	74.5	14.5	15.5	N
TR034	Luoman	Beijing	27.939	108.831	11	291.6	-75.9	111.6	81.5	13.0	13.4	R
TR035	Luoman	Berkeley	27.954	108.821	19	42.4	68.4	42.4	76.6	14.9	6.0	N
TR037	Luoman	Beijing	27.946	108.829	17	202.1	-86.3	22.1	87.8	17.2	5.3	R
TR039	Luoman	Beijing	27.946	108.829	9	136.8	-78.1	316.8	82.8	21.2	6.8	R
TR042	Luoman	Berkeley	27.943	108.839	14	131.5	-71.9	311.5	78.9	11.5	13.0	R

Notes:
(1) All directions are for the high temperature component.
(2) $\mathbf{dec}_{1.0}$ and $\mathbf{inc}_{1.0}$ refer to the declination and inclination of the mean tilt-corrected direction, without correcting for polarity or inclination shallowing.
(3) $\mathbf{dec}_{0.6}$ and $\mathbf{inc}_{0.6}$ refer to the declination and inclination of the mean tilt-corrected direction, after correcting for polarity and inclination shallowing using a flattening factor of 0.6.
(4) For the **polarity**, we interpret the mean directions with a positive inclination as normal polarity (N), and the mean directions with a negative inclination as reverse polarity (R).

Table 2. Summary of CA-ID-TIMS $^{206}Pb/^{238}U$ dates from tuffs developed in this study.

sample	latitude °N	longitude °E	section	stratigraphic height (m)	$^{206}Pb/^{238}U$ date (Ma)	error (2σ) X	Y	Z	MSWD	n	N
Xiajiang Group of the Fanjingshan region (Guizhou province)											
H2-470	27.99396	108.79792	Hongzixi	1586.2	815.73	0.18	0.28	0.92	1.6	6	16
L1-27	27.93856	108.83107	Luoman	1752.3	814.19	0.21	0.31	0.92	1.7	5	9
L4-2	27.94335	108.83931	Luoman	1815.5	813.06	0.35	0.48	1.0	1.8	3	4
H3-60	28.01002	108.80240	Hongzixi	2622.4	809.52	0.50	0.62	1.1	1.9	6	10
QR-74	27.86578	108.82076	Kuaichang	2850.3	811.47	0.67	0.77	1.2	1.9	3	6
H3-8	28.02468	108.81506	Hongzixi	3389.3	804.56	0.39	0.52	1.0	0.6	3	4
Madiyi Formation in the Zhijiang region (Hunan province)											
ZJ-B	27.5	109.6	-	-	804.90	0.36	0.49	0.99	0.9	5	6
Liantuo Formation in the Three Gorges region (Hubei province)											
FDM14-1	30.8527	111.1512	-	-	779.52	0.26	0.38	0.92	2.0	8	16

Notes:
(1) **stratigraphic height** is the estimated composite stratigraphic height derived from correlation of individually measured sections based on aligning the bounding unconformities of the Xiajiang Group and the geochronologic results.
(2) For the **errors**, **X** is the internal (analytical) uncertainty in the absence of external or systematic errors, **Y** is the uncertainty incorporating the U-Pb tracer calibration error, and **Z** is the uncertainty including X and Y, as well as ^{238}U decay constant uncertainty (0.108%; Jaffey et al., 1971). This Z error needs to be utilized when comparing to dates developed using other decay systems (e.g., $^{40}Ar/^{39}Ar$, ^{187}Re-^{187}Os).
(3) **MSWD** is the mean square of weighted deviates
(4) **n** is the number of individual zircon dates included in the calculated weighted sample mean date.
(5) **N** is the total number of individual zircons analyzed.
(6) Data for individual zircons are provided in the Supporting Information.

Table 3. Neoproterozoic paleomagnetic poles for South China.

pole	nominal age (Ma)	age method	site lat.	site lon.	pole lat.	pole lon.	A_{95}	f	pole ref.	age ref.	note
Yanbian dikes	824±6	SIMS	26.9	101.5	45.1	130.4	19.0	1.0	Niu et al. (2016)	Niu et al. (2016)	(2)
Xiaofeng dikes	821.64±0.2	CA-ID-TIMS	31.0	111.2	26.1	82.1	14.6	1.0	Jing et al. (2020)	Wang et al. (2016b)	(3)
Xiajiang Group	816–810	CA-ID-TIMS	27.9	108.8	42.7	104.0	8.1	0.6	this study	this study	-
Madiyi Formation	804.90±0.99	CA-ID-TIMS	27.5	109.6	34.7	82.0	6.7	0.6	Xian et al. (2020)	this study	(4)
Chengjiang Formation	799.5±8.4	SIMS	25.1	102.4	29.7	75.3	7.9	0.6	Jing et al. (2020)	Jing et al. (2020)	(5)
lower Liantuo Formation (Member 1)	∼779.52±0.92	CA-ID-TIMS	30.8	110.9	24.9	136.4	6.6	0.6	Jing et al. (2021)	this study	(5)
upper Liantuo Formation (Member 2)	≤779.52±0.92	CA-ID-TIMS	30.8	111.1	19.6	144.4	4.2	0.6	Jing et al. (2015)	this study	(5)

Notes:
(1) **f** is the flattening factor, where f=1 indicates no inclination shallowing and f=0 indicates a completely flattened direction.
(2) Located within mobile belt.
(3) Pole recalculated after Li et al. (2004).
(4) Pole converted from specimen to site mean in this study.
(5) Inclination correction applied in this study.

Table 4. 900-700 Ma paleomagnetic poles for cratons proximal to South China.

pole	nominal age (Ma)	site lat.	site lon.	pole lat.	pole lon.	A_{95}	f	ref.	grade
Laurentia									
Gunbarrel dikes	778^{+2}_{-2}	44.8	248.7	9.1	138.2	12.0	1.0	Eyster et al. (2019)	B
Uinta Mountain Group	760^{+6}_{-10}	40.8	250.7	1.2	161.8	4.7	0.6	Weil et al. (2006)	B
Carbon Canyon	757^{+7}_{-7}	36.1	248.2	-0.5	166	9.7	0.5	Eyster et al. (2019)	NR
Carbon Butte/Awatubi	751^{+8}_{-8}	35.2	248.5	14.2	163.8	3.5	0.9	Eyster et al. (2019)	NR
Franklin event grand mean	724^{+3}_{-3}	73.0	275.4	6.7	162.1	3.0	1.0	Denyszyn et al. (2009)	A
Svalbard									
Lower Grusdievbreen Formation	815^{+5}_{-5}	79.0	18.0	19.6	204.9	10.9	1.0	Maloof et al. (2006)	B
Upper Grusdievbreen Formation	802^{+8}_{-7}	78.9	18.2	-1.1	252.6	6.2	1.0	Maloof et al. (2006)	B
Svanbergfjellet Formation	785^{+5}_{-5}	78.5	18.0	25.9	226.8	5.8	1.0	Maloof et al. (2006)	B
Siberia									
Kitoi Cryogenian dikes	758^{+4}_{-4}	52.3	102.8	1.1	21.8	5.6	1.0	Pisarevsky et al. (2013)	A
Australia									
Browne Formation	855^{+45}_{-45}	-25.0	123.8	34.3	138.0	8.4	0.6	Pisarevsky et al. (2007)	B
Johnny's Creek siltstones	760^{+30}_{-30}	-24.0	133.5	7.1	92.6	14.7	0.6	Swanson-Hysell et al. (2012)	B
Mundine Well dikes combined	755^{+3}_{-3}	-25.5	115.0	45.3	135.4	4.1	1.0	Wingate and Giddings (2000)	A
India									
Malani Igneous Suite combined	752^{+18}_{-18}	25.3	72.6	69.4	78.6	6.0	1.0	Meert et al. (2013)	A

Notes:
(1) **grade** is the quality of the pole as assessed by the Nordic Paleomagnetism Workshops (Evans et al., 2021). 'A' refers to poles that are considered to provide essential constraints given their high quality. 'B' refers to poles that are likely high quality, but retain some ambiguity about their age or direction. 'NR' refers to poles that were not rated at the Nordic Paleomagnetism Workshops.
(2) **f** is the flattening factor, where f=1 indicates no inclination shallowing and f=0 indicates a completely flattened direction. An inclination correction using $f = 0.6$ has been applied to all paleomagnetic poles derived from sedimentary rocks, with the exception of the Carbon Canyon and Carbon Butte/Awatubi poles, for which we retain the flattening factor preferred by Eyster et al. (2019), and the poles from Svalbard, which were derived from carbonates that experienced early cementation, and therefore are unlikely to be affected by inclination shallowing related to compaction (Maloof et al., 2006).

FIGURES

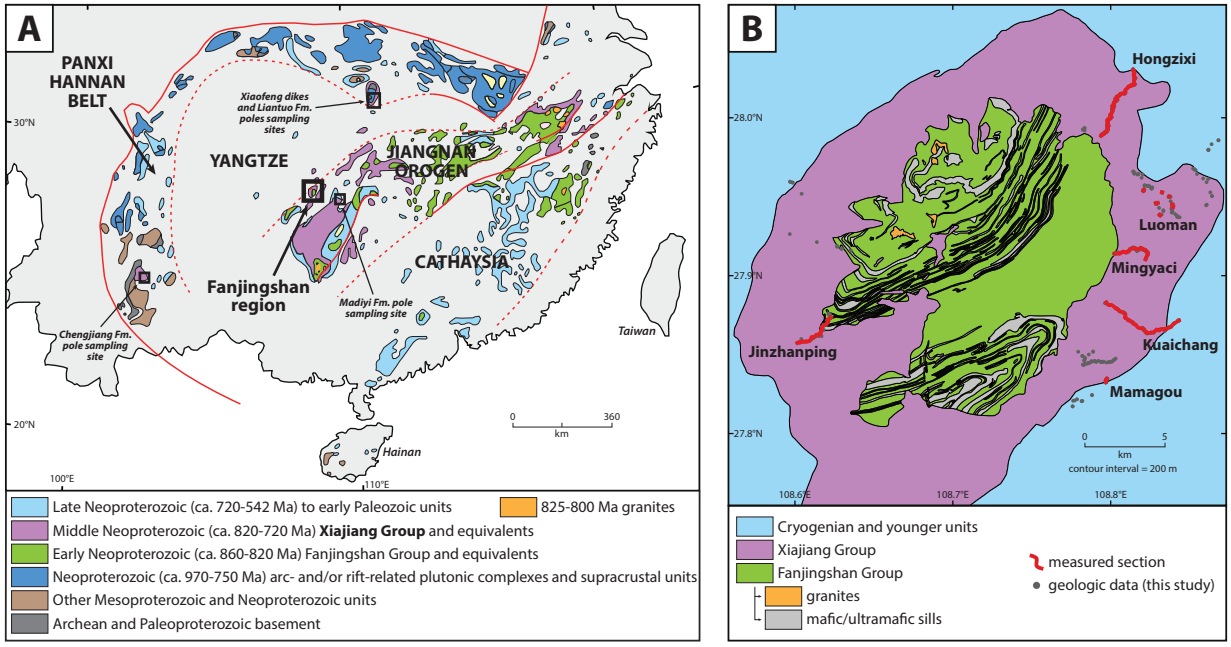

Figure 1. **A)** Summary geologic map of South China, adapted from Cawood et al. (2017), showing the Fanjingshan region from where the Xiajiang Group pole is developed in this study, as well as the localities where other Neoproterozoic poles are developed (Table 3). **B)** Geologic map of the Fanjingshan region. The distribution of volcanic units within the Fanjingshan Group and the contact between the Fanjingshan and Xiajiang groups were adapted from Wang et al. (2016a). Both the sedimentary and volcanic units of the Fanjingshan Group were folded, uplifted, and eroded prior to Xiajiang Group deposition. The contact between the Xiajiang Group and the overlying Cryogenian units was adapted from Zhao et al. (2011). Unit boundaries were adjusted to be consistent with our geologic data where available. Red lines show the location of the measured stratigraphic sections in Figure 2. Note that the Luoman section consists of seven individually measured sections that were correlated to each other based on local bedding and elevation measurements.

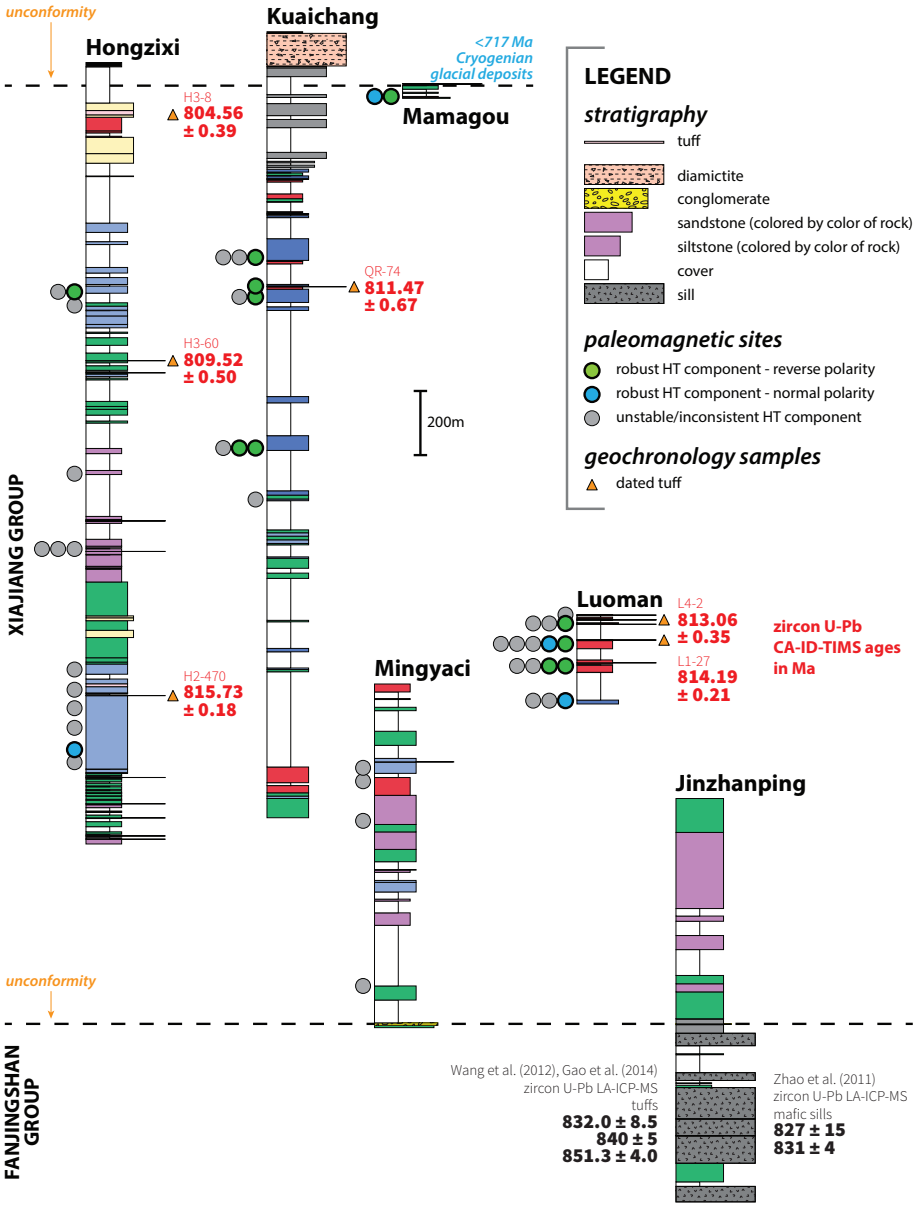

Figure 2. Stratigraphic sections measured in the Fanjingshan region. Locations of measured sections are shown in Figure 1. The colors are associated with the color of the sedimentary rocks. U-Pb CA-ID-TIMS dates from the Xiajiang Group are from this study and are shown at the stratigraphic levels where the tuffs were collected. The dates from the Fanjingshan Group are not from the section shown, but are from other studies of the rocks elsewhere in the region.

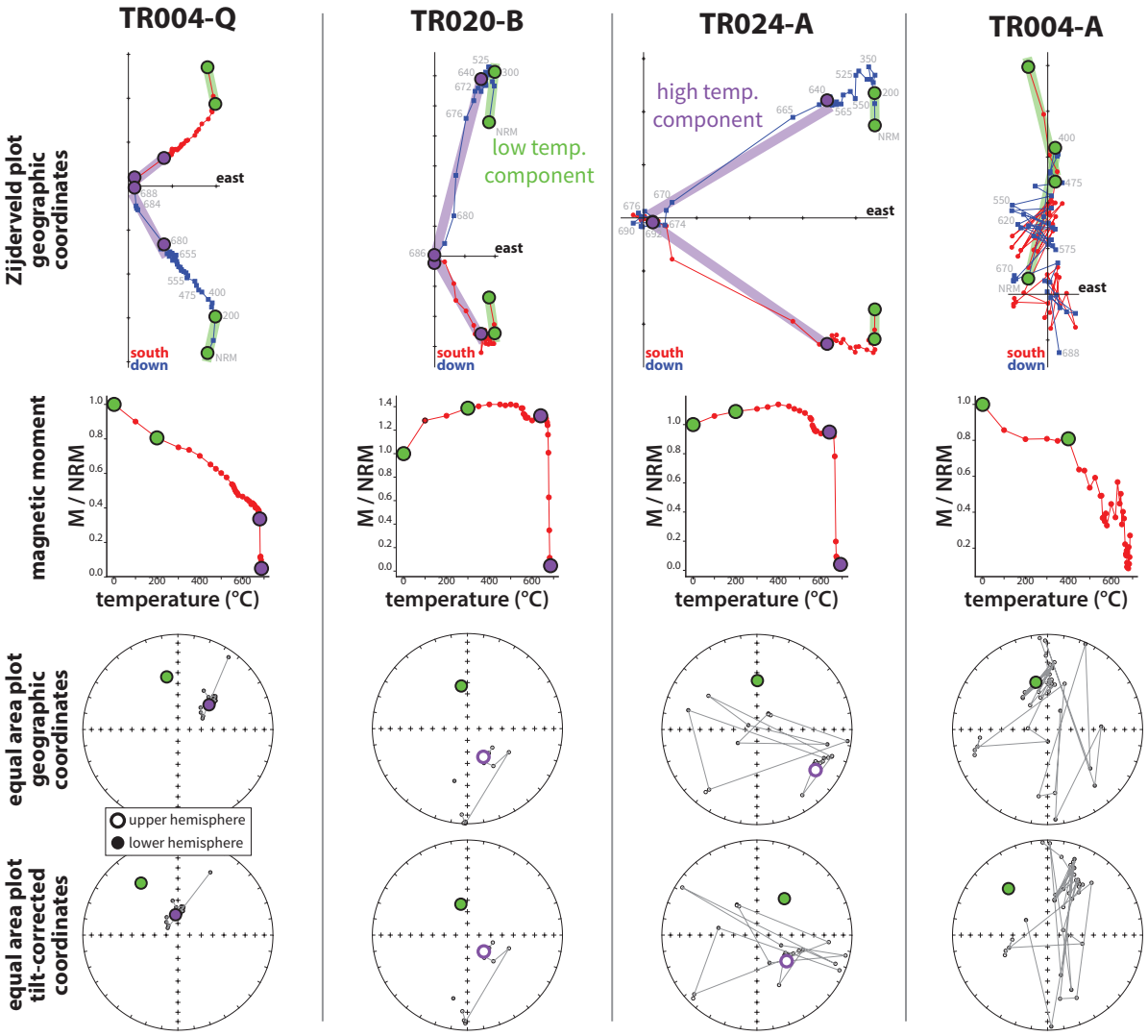

Figure 3. Thermal demagnetization results. Specimens TR004-Q, TR020-B, and TR024-A exhibit magnetic behaviour typical of specimens that yield a stable and consistent high temperature component. Specimen TR004-Q exhibits magnetic behaviour typical of specimens that do not yield a stable high temperature component. In the Zijderveld plots, the specimen magnetizations at a given thermal demagnetization step (grey numbers) are shown (NRM = natural remanent magnetization). Fits to the low and high temperature components are shown in green and purple respectively. Note that the Zijderveld plots and the upper equal area plots are in geographic coordinates, whereas the lower equal area plot is in tilt-corrected coordinates.

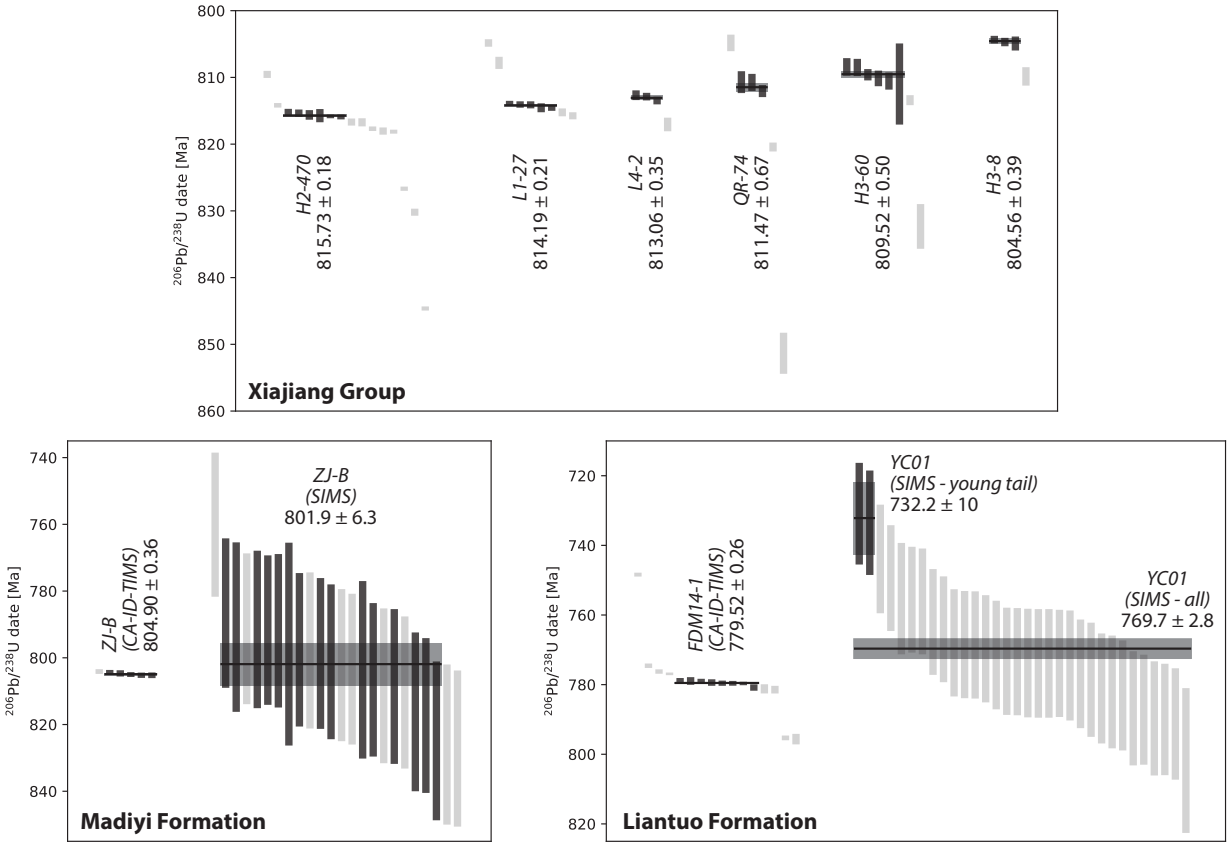

Figure 4. 2σ uncertainty of CA-ID-TIMS U-Pb dates for zircons analyzed in this study. The previously reported SIMS dates for sample ZJ-B of the Madiyi Formation (Xian et al., 2020) and sample YC01 of the Liantuo Formation (Lan et al., 2015) are also shown. For sample YC01, we show the weighted mean dates that result from isolating the two youngest zircons (as is preferred in Lan et al., 2015) and from including all of the zircons. Solid vertical bars indicate zircons that are included in the calculation of the weighted mean date. Faded vertical bars indicate zircons interpreted to have been inherited or affected by Pb or U loss, and are excluded in the calculation of the weighted mean date. Measurement data are and concordia diagrams are shown in the Supporting Information.

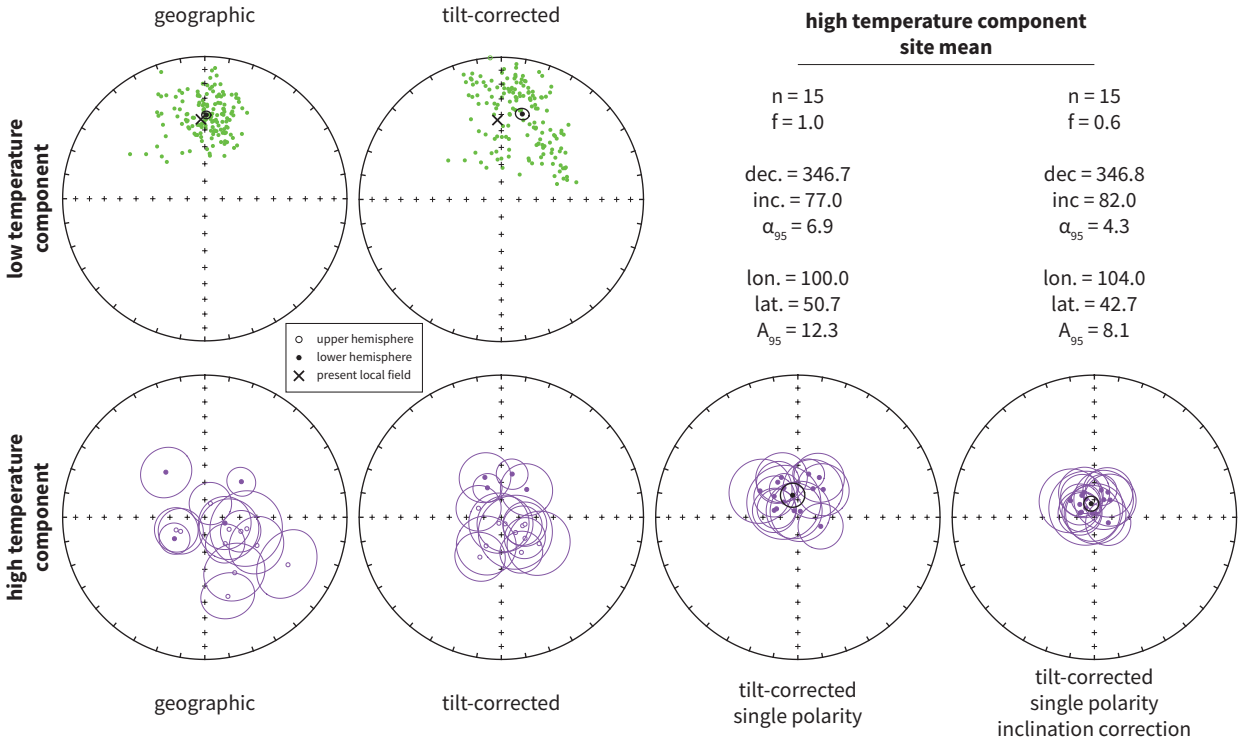

Figure 5. Paleomagnetic results for sites that yielded specimens with stable and consistent high temperature components in the Xiajiang Group of the Fanjingshan region (Table 1). For the low temperature component, each point represents an individual specimen. For the high temperature component, each point and associated uncertainty ellipse represents the specimen mean for individual sites. The reported site means are the means of these specimen means.

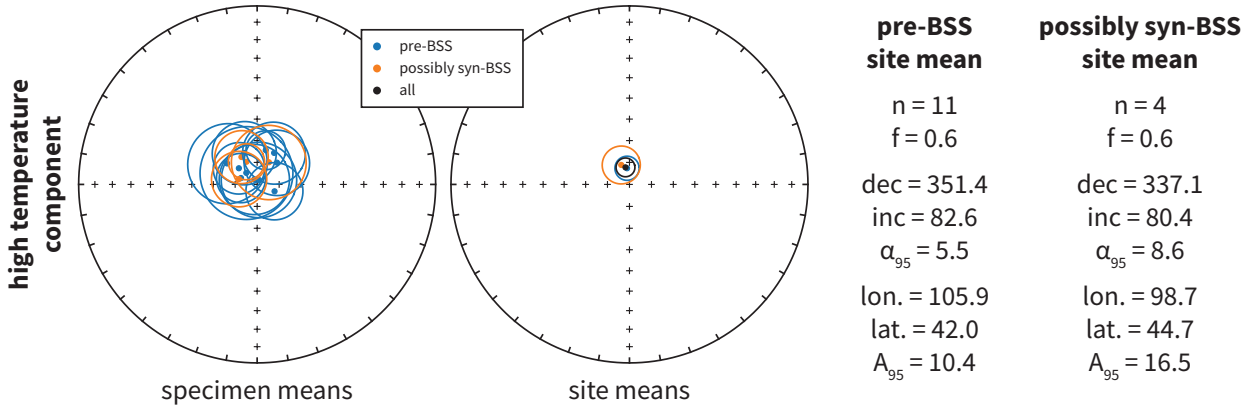

Figure 6. Comparison of the high temperature component from sites that are unambiguously constrained by the geochronology to be pre-Bitter Springs Stage and sites that could be syn-Bitter Springs Stage (Fig. 2). The angular difference between the two site mean directions is 3.0°.

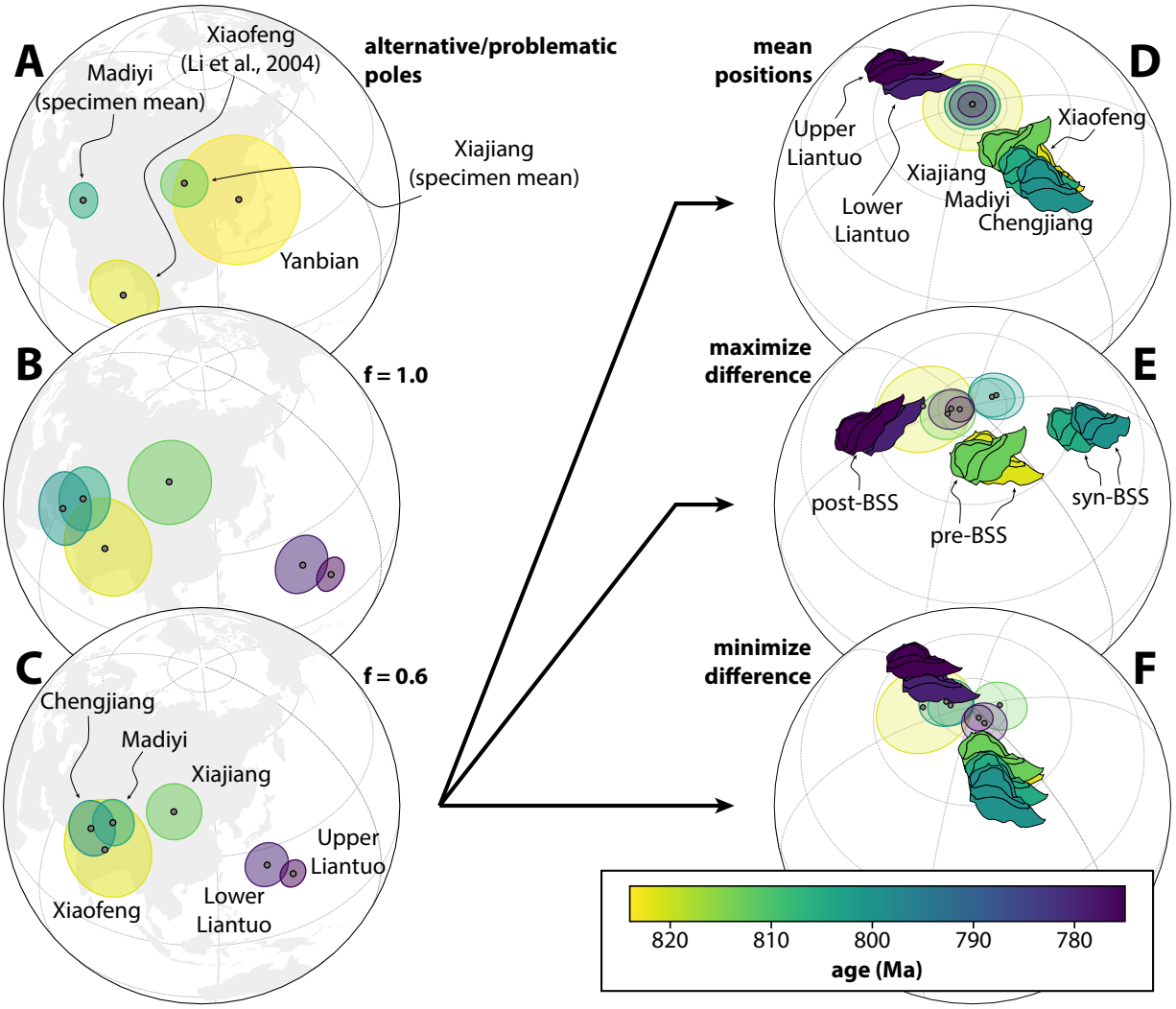

Figure 7. Tonian apparent polar wander paths (APWPs) and paleogeographic models for South China. **A)** Alternative/problematic paleomagnetic poles. See text for details. **B)** APWP using the preferred poles, with poles derived from sedimentary rocks shown as site means without an inclination correction. **C)** APWP using the preferred poles, with poles derived from sedimentary rocks shown as site means with an inclination correction. ($f = 0.6$). **D)** Paleogeographic model based on the preferred APWP in C. South China is reconstructed using the means of the poles. **E)** Paleogeographic model based on the preferred APWP with South China reconstructed to maximize the difference in position between the pre-, syn-, and post-Bitter Springs Stage (BSS) poles as permitted by the A_{95} uncertainties. **F)** Paleogeographic model based on the preferred APWP with South China reconstructed to minimize the difference in position permitted by the A_{95} uncertainties of all poles.

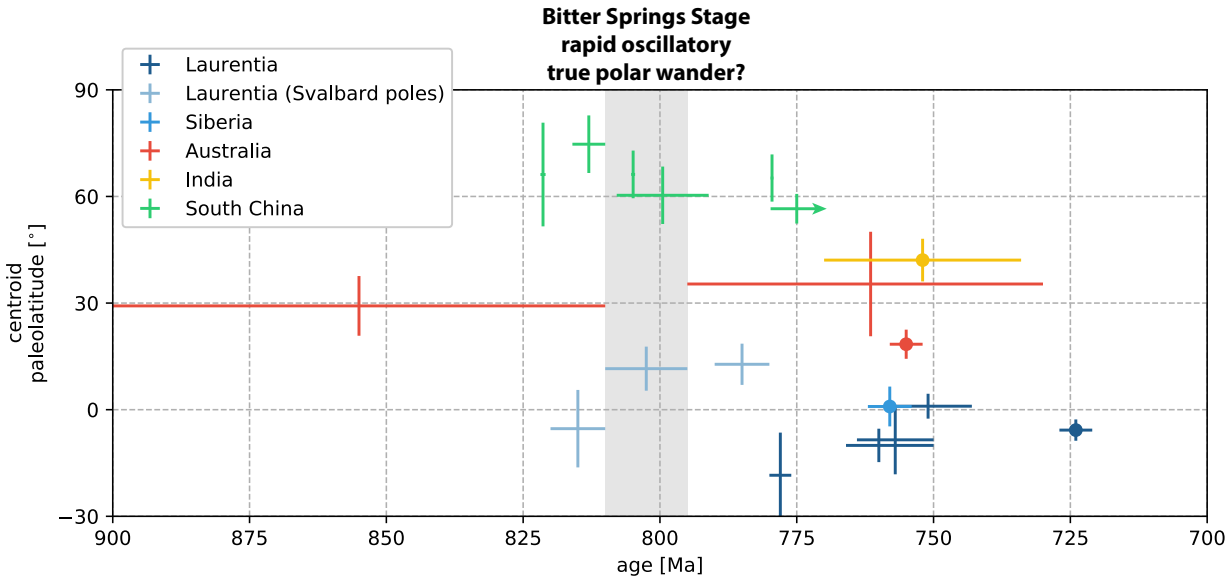

Figure 8. Paleolatitudes of points in the center of South China and other cratons implied by available paleomagnetic poles shown with age and paleolatitude uncertainty (Tables 3 and 4). The light blue 'Laurentia (Svalbard poles)' are for the centroid of Laurentia reconstructed using Svalbard poles with Svalbard rotated back to Laurentia. Points with a circle in the center indicate paleomagnetic poles that were given an 'A' rating by the Nordic Paleomagnetism Workshops. The grey bar indicates the timing of the ca. 810-795 Ma Bitter Springs Stage which is hypothesized to have been bracketed by rapid true polar wander rotations.

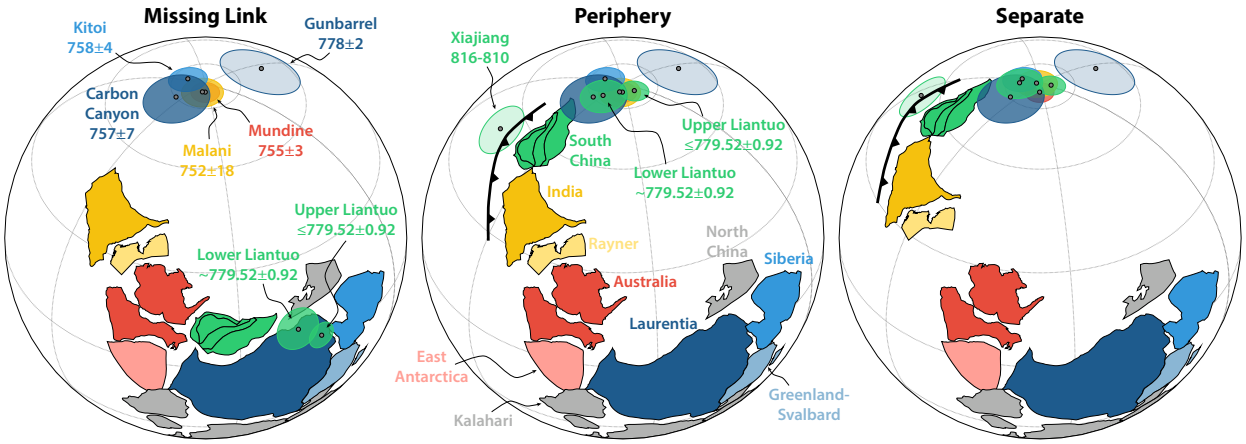

Figure 9. Paleogeographic reconstructions for Rodinia at 755 Ma. The Missing Link model places South China at low latitudes between Australia and Laurentia, which is inconsistent with both the paleomagnetic data as well as the tectonic context of South China. The Periphery model instead places South China at high latitudes connected to India, which satisfies the ca. 755 Ma and 780 Ma paleomagnetic data and allows for an active margin along the Panxi-Hannan Belt at this time. In order to satisfy ca. 821-805 Ma paleomagnetic data from South China, anticlockwise rotation of the entire Rodinia supercontinent from ca. 821-805 Ma to ca. 780 Ma is required in this Periphery model. The Separate model disconnects South China-India-Rayner from Rodinia. The Euler rotation parameters for South China relative to India in the Periphery and Separate models are (6.72° N, 77.69° E, 67.96°). Blocks that are not directly relevant to the relationship between South China and Rodinia are shown in grey.

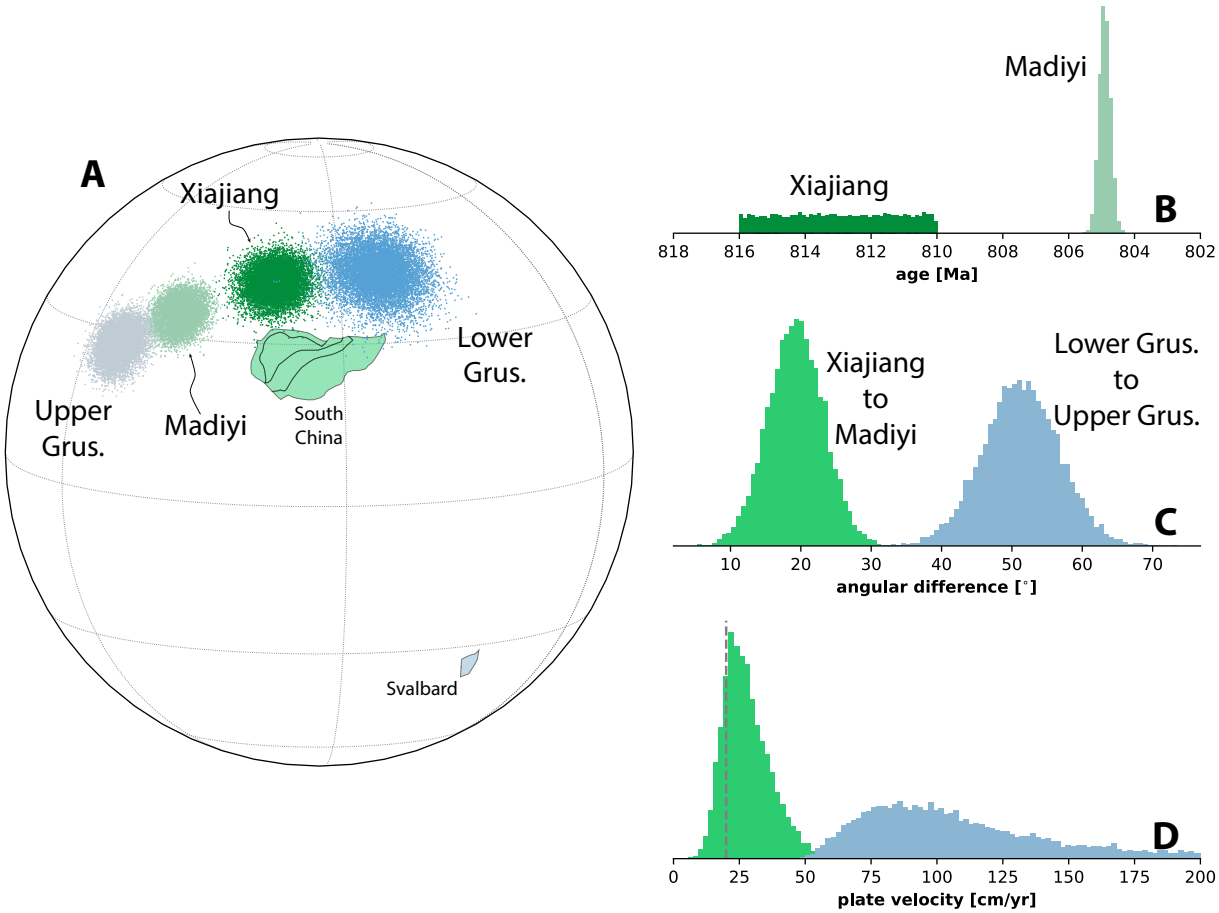

Figure 10. Results of Monte Carlo analysis of hypothesized ca. 810 Ma rapid true polar wander motion. **A)** Virtual geomagnetic poles (VGPs) for the Xiajiang Group, Madiyi Formation, and Lower and Upper Grusdievbreen Formation paleomagnetic poles randomly sampled from Fisherian distributions ($n = 10,000$). South China is shown in its present day location, and Svalbard is rotated such that the 4 poles lie along a great circle. **B)** Ages of the Xiajiang Group and Madiyi Formation poles randomly sampled from uniform and Gaussian distributions respectively. **C)** Angular difference between randomly selected VGP pairs in A. **D)** Plate velocity of South China implied by A and B, and the plate velocity of Svalbard implied by A and assuming that the Upper Grusdievbreen Formation pole is 1–10 m.y. younger than the Lower Grusdievbreen Formation pole. The dashed vertical line is the ∼20 cm/yr plate velocity limit suggested by Conrad and Hager (2001) and Zahirovic et al. (2015).

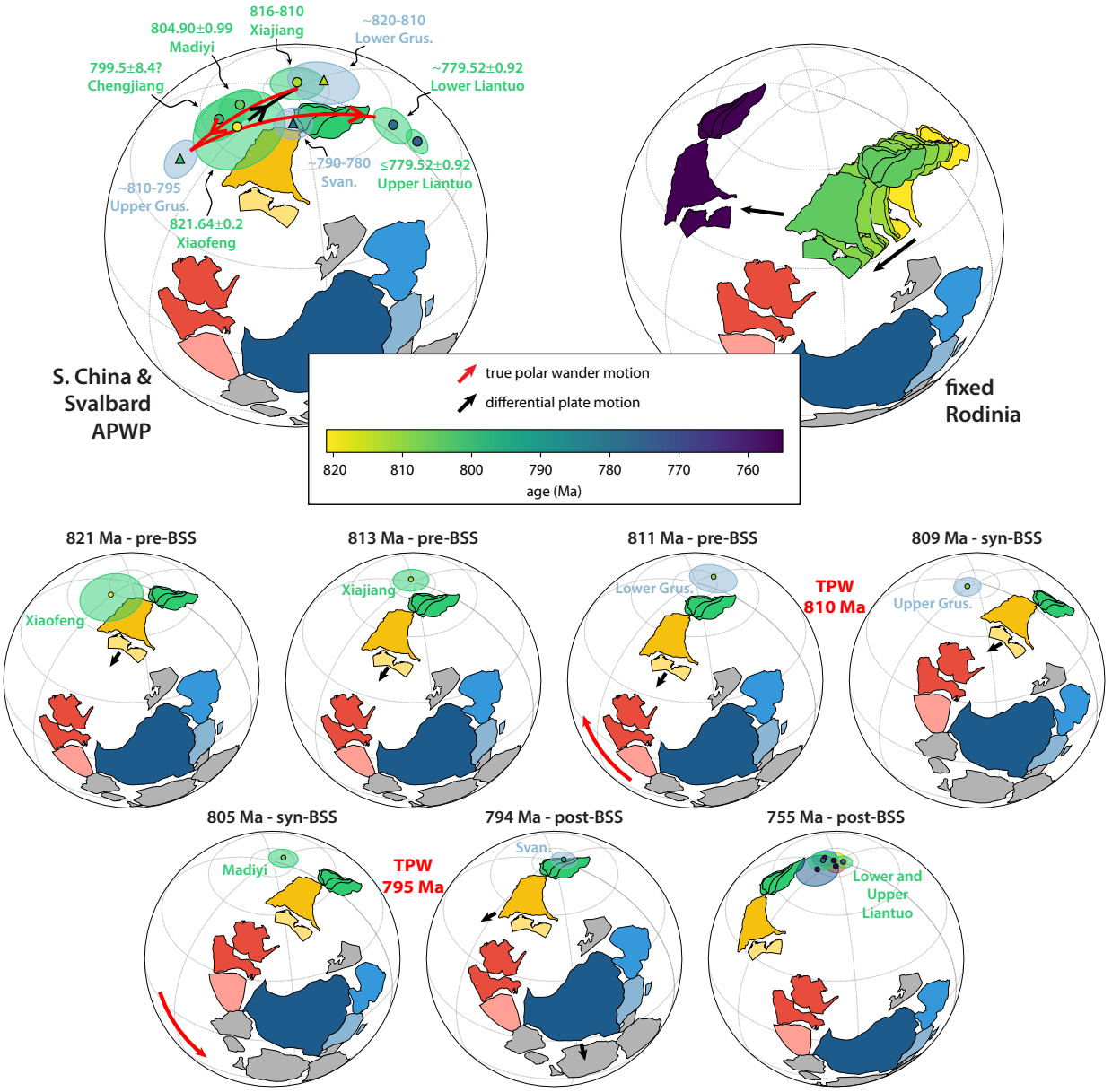

Figure 11. Continuous paleogeographic model if Tonian paleomagnetic poles from South China are interpreted as recording differential plate motion superimposed upon Bitter Springs Stage (BSS) true polar wander (TPW). In the upper left, the tectonic blocks are shown in a ca. 813 Ma reconstruction, and the apparent polar wander paths (APWPs) of South China and Svalbard are aligned along two great circles. In the upper right, Rodinia (Laurentia + associated cratons) is fixed in a ca. 755 Ma reconstruction to show the differential motion of South China-India-Rayner relative to Rodinia. The seven lower reconstructions show pre-, syn-, and post-BSS reconstructions in a celestial reference frame. Note that differential plate motion of South China-India-Rayner continues through ca. 810 Ma rapid TPW defined by the Lower and Upper Grusdievbreen Formation poles of Svalbard. Euler rotations for this paleogeographic model are shown in Table S9.

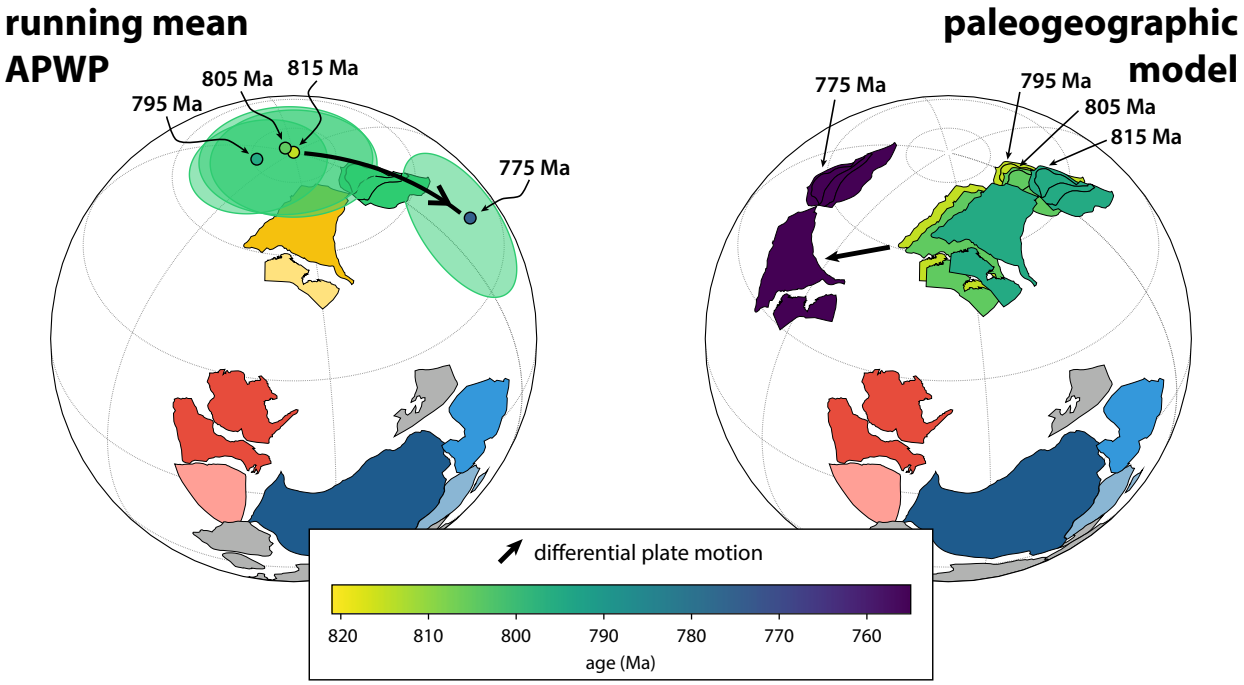

Figure 12. Paleogeographic model if paleomagnetic data from Svalbard are interpreted as problematic and removed as constraints, resulting in a model that does not incorporate Bitter Springs Stage (BSS) true polar wander (TPW). A running mean approach (10 million year time steps with 20 million year windows; Table S10) is used to produce the apparent polar wander path (APWP) for South China, as is done for Phanerozoic APWPs (Torsvik et al., 2012). This APWP is parsimoniously interpreted to represent a stable South China-India-Rayner at high latitudes ca. 815 to 795 Ma that subsequently traverses the north pole ca. 795 to 775 Ma. In the left panel the tectonic blocks are shown in a ca. 815 Ma reconstruction with the running mean APWP, and in the right panel a paleogeographic model is shown where South China-India-Rayner are reconstructed using the means of the running mean poles.

References

Ashwal, L., Solanki, A., Pandit, M., Corfu, F., Hendriks, B., Burke, K., and Torsvik, T., 2013, Geochronology and geochemistry of Neoproterozoic Mt. Abu granitoids, NW India: Regional correlation and implications for Rodinia paleogeography: Precambrian Research, vol. 236, pp. 265–281, doi:10.1016/j.precamres.2013.07.018.

Bilardello, D., 2016, The do's and don'ts of inclination shallowing corrections: IRM Quarterly, vol. 26, pp. 1–11.

Bowring, S. A., Grotzinger, J. P., Condon, D. J., Ramezani, J., Newall, M. J., and Allen, P. A., 2007, Geochronologic constraints on the chronostratigraphic framework of the Neoproterozoic Huqf Supergroup, Sultanate of Oman: American Journal of Science, vol. 307, pp. 1097–1145, doi:10.2475/10.2007.01.

Bureau of Geology and Mineral Resources of Guizhou Province, 1984, Regional geology of Guizhou Province: Geological Publishing House, Beijing.

Cambiotti, G., Ricard, Y., and Sabadini, R., 2010, Ice age True Polar Wander in a compressible and non-hydrostatic Earth: Geophysical Journal International, vol. 183, pp. 1248–1264, doi:10.1111/j.1365-246x.2010.04791.x.

Cawood, P. A., Wang, Y., Xu, Y., and Zhao, G., 2013, Locating South China in Rodinia and Gondwana: A fragment of greater India lithosphere?: Geology, vol. 41, pp. 903–906, doi:10.1130/G34395.1.

Cawood, P. A., Zhao, G., Yao, J., Wang, W., Xu, Y., and Wang, Y., 2017, Reconstructing South China in Phanerozoic and Precambrian supercontinents: Earth-Science Reviews, doi:10.1016/j.earscirev.2017.06.001.

Chan, N.-H., Mitrovica, J. X., Daradich, A., Creveling, J. R., Matsuyama, I., and Stanley, S., 2014, Time-dependent rotational stability of dynamic planets with elastic lithospheres: Journal of Geophysical Research: Planets, vol. 119, pp. 169–188, doi:10.1002/2013je004466.

Condon, D. J., Schoene, B., McLean, N. M., Bowring, S. A., and Parrish, R. R., 2015, Metrology and traceability of U-Pb isotope dilution geochronology (EARTHTIME tracer calibration part I): Geochimica et Cosmochimica Acta, vol. 164, pp. 464–480, doi:10.1016/j.gca.2015.05.026.

Conrad, C. P. and Hager, B. H., 2001, Mantle convection with strong subduction zones: Geophysical Journal International, vol. 144, pp. 271–288, doi:10.1046/j.1365-246x.2001.00321.x.

Creveling, J. R., Mitrovica, J. X., Chan, N.-H., Latychev, K., and Matsuyama, I., 2012, Mechanisms for oscillatory true polar wander: Nature, vol. 491, pp. 244–248, doi:10.1038/nature11571.

Denyszyn, S. W., Halls, H. C., Davis, D. W., and Evans, D. A., 2009, Paleomagnetism and U-Pb geochronology of Franklin dykes in High Arctic Canada and Greenland: a revised age and paleomagnetic pole constraining block rotations in the Nares Strait region: Canadian Journal of Earth Sciences, vol. 46, pp. 689–705, doi:10.1139/E09-042.

Dong, Y., Liu, X., Santosh, M., Chen, Q., Zhang, X., Li, W., He, D., and Zhang, G., 2012, Neoproterozoic accretionary tectonics along the northwestern margin of the Yangtze Block, China: Constraints from zircon U-Pb geochronology and geochemistry: Precambrian Research, vol. 196-197, pp. 247–274, doi:10.1016/j.precamres.2011.12.007.

Duebendorfer, E. M., 2002, Regional correlation of Mesoproterozoic structures and deformational events in the Albany-Fraser orogen, Western Australia: Precambrian Research, vol. 116, pp. 129–154, doi:10.1016/s0301-9268(02)00017-7.

Dunlop, D. J. and Özdemir, Ö., 2001, Rock magnetism: fundamentals and frontiers, vol. 3: Cambridge University Press.

Ernst, R. E., Hamilton, M. A., Söderlund, U., Hanes, J. A., Gladkochub, D. P., Okrugin, A. V., Kolotilina, T., Mekhonoshin, A. S., Bleeker, W., LeCheminant, A. N., Buchan, K. L., Chamberlain, K. R., and Didenko, A. N., 2016, Long-lived connection between southern Siberia and northern Laurentia in the Proterozoic: Nature Geoscience, vol. 9, pp. 464–469, doi:10.1038/ngeo2700.

Evans, D., Pesonen, L., Eglington, B., Elming, S.-Å., Gong, Z., Li, Z.-X., McCausland, P., Meert, J., Mertanen, S., Pisarevsky, S., Pivarunas, A., Salminen, J., Swanson-Hysell, N., Torsvik, T., Trindade, R., Veikkolainen, T., and Zhang, S., 2021, An expanding list of reliable paleomagnetic poles for Precambrian tectonic reconstructions: *In* Pesonen, L., Salminen, J., Elming, S.-Å., Evans, D., and Veikkolainen, T., eds., Ancient Supercontinents and the Paleogeography of the Earth, Elsevier.

Evans, D. A., 2003, True polar wander and supercontinents: Tectonophysics, vol. 362, pp. 303–320, doi:10.1016/s0040-1951(02)000642-x.

Evans, D. A., Veselovsky, R. V., Petrov, P. Y., Shatsillo, A. V., and Pavlov, V. E., 2016, Paleomagnetism of Mesoproterozoic margins of the Anabar Shield: A hypothesized billion-year partnership of Siberia and northern Laurentia: Precambrian Research, vol. 281, pp. 639–655, doi:10.1016/j.precamres.2016.06.017.

Evans, D. A. D., Li, Z. X., Kirschvink, J. L., and Wingate, M. T. D., 2000, A high-quality mid-Neoproterozoic paleomagnetic pole from South China, with implications for ice ages and the breakup configuration of Rodinia: Precambrian Research, vol. 100, pp. 313–334, doi:10.1016/S0301-9268(99)00079-0.

Eyster, A., Weiss, B. P., Karlstrom, K., and Macdonald, F. A., 2019, Paleomagnetism of the Chuar Group and evaluation of the late Tonian Laurentian apparent polar wander path with implications for the makeup and breakup of Rodinia: GSA Bulletin, doi:10.1130/b32012.1.

Fisher, D., 1974, Some more remarks on polar wandering: Journal of Geophysical Research, vol. 79, pp. 4041–4045, doi:10.1029/jb079i026p04041.

Gao, L., Chen, J., Dai, C., Ding, X., Wang, X., Liu, Y., Wang, M., and Zhang, H., 2014, SHRIMP zircon U-Pb dating of tuff in Fanjingshan Group and Xiajiang Group from Guizhou and Hunan Provinces and its stratigraphic implications: Geological Bulletin of China, vol. 33, pp. 949–959.

Gao, L., Yang, Z., Tong, Y., Wang, H., An, C., and Zhang, H., 2017, Cenozoic clockwise rotation of the Chuan Dian Fragment, southeastern edge of the Tibetan Plateau: Evidence from a new paleomagnetic study: Journal of Geodynamics, vol. 112, pp. 46–57, doi:10.1016/j.jog.2017.10.001.

Gao, L.-Z., Dai, C.-G., Ding, X.-Z., Wang, M., Liu, Y.-X., Wang, X.-H., and Chen, J.-S., 2011, SHRIMP U-Pb dating of intrusive alaskite in the Fanjigshan Group and alaskite basal conglomerates: constraints on the deposition of the Xiajiang Group: Geology in China, vol. 38.

Gao, L. Z., Dai, C. G., Liu, Y. X., Wang, M., Wang, X. H., Chen, J. S., and Ding, X. Z., 2010, Zircon SHRIMP U-Pb dating of the tuffaceous bed of Xiajiang Group in Guizhou Province and its stratigraphic implication: Geology in China, vol. 37, pp. 1071–1080.

Geng, Y.-S., 2015, Neoproterozoic Era of South China Craton: Springer Geology, pp. 263–301, doi:10.1007/978-3-662-47885-1_7.

Göğüş, O. H., 2015, Rifting and subsidence following lithospheric removal in continental back arcs: Geology, vol. 43, pp. 3–6, doi:10.1130/g36305.1.

Gold, T., 1955, Instability of the Earth's axis of rotation: Nature, vol. 175, pp. 526–529, doi:10.1038/175526a0.

Goodge, J. W. and Fanning, C. M., 2010, Composition and age of the East Antarctic Shield in eastern Wilkes Land determined by proxy from Oligocene-Pleistocene glaciomarine sediment and Beacon Supergroup sandstones, Antarctica: Geological Society of America Bulletin, vol. 122, pp. 1135–1159, doi:10.1130/b30079.1.

908 Goodge, J. W., Vervoort, J. D., Fanning, C. M., Brecke, D. M., Farmer, G. L., Williams, I. S., Myrow, P. M., and
909 DePaolo, D. J., 2008, A positive test of East Antarctica-Laurentia juxtaposition within the Rodinia
910 supercontinent: Science, vol. 321, pp. 235–240, doi:10.1126/science.1159189.

911 Halverson, G. P., Maloof, A. C., Schrag, D. P., Dudás, F. Ö., and Hurtgen, M., 2007, Stratigraphy and
912 geochemistry of a ca 800 Ma negative carbon isotope interval in northeastern Svalbard: Chemical Geology, vol.
913 237, pp. 5–27, doi:10.1016/j.chemgeo.2006.06.013.

914 Hildebrand, R. S., 1988, Implications of ash dispersal for tectonic models with an example from Wopmay orogen:
915 Geology, vol. 16, pp. 1089–1091, doi:10.1130/0091-7613(1988)016⟨1089:ioadft⟩2.3.co;2.

916 Jackson, M. and Swanson-Hysell, N. L., 2012, Rock magnetism of remagnetized carbonate rocks: another look:
917 Geological Society, London, Special Publications, vol. 371, pp. 229–251, doi:10.1144/sp371.3.

918 Jaffey, A. H., Flynn, K. F., Glendenin, L. E., Bentley, W. C., and Essling, A. M., 1971, Precision measurement of
919 half-lives and specific activities of ^{235}U and ^{238}U: Phys. Rev. C, vol. 4, pp. 1889–1906,
920 doi:10.1103/PhysRevC.4.1889.

921 Jiang, Z., Liu, Q., Dekkers, M. J., Tauxe, L., Qin, H., Barrón, V., and Torrent, J., 2015, Acquisition of chemical
922 remanent magnetization during experimental ferrihydrite-hematite conversion in Earth-like magnetic
923 field-implications for paleomagnetic studies of red beds: Earth and Planetary Science Letters, vol. 428, pp. 1 –
924 10, doi:10.1016/j.epsl.2015.07.024.

925 Jing, X., Evans, D. A., Yang, Z., Tong, Y., Xu, Y., and Wang, H., 2021, Inverted South China: A novel
926 configuration for Rodinia and its breakup: Geology, doi:10.1130/g47807.1.

927 Jing, X., Yang, Z., Evans, D. A., Tong, Y., Xu, Y., and Wang, H., 2020, A pan-latitudinal Rodinia in the Tonian
928 true polar wander frame: Earth and Planetary Science Letters, pp. 1–14, doi:10.1016/j.epsl.2019.115880.

929 Jing, X.-q., Yang, Z., Tong, Y., and Han, Z., 2015, A revised paleomagnetic pole from the mid-Neoproterozoic
930 Liantuo Formation in the Yangtze block and its paleogeographic implications: Precambrian Research, vol. 268,
931 pp. 194–211, doi:10.1016/j.precamres.2015.07.007.

932 Katz, B., Elmore, R., and Engel, M., 1998, Authigenesis of magnetite in organic-rich sediment next to a dike:
933 implications for thermoviscous and chemical remagnetizations: Earth and Planetary Science Letters, vol. 163, pp.
934 221–234, doi:10.1016/s0012-821x(98)00189-7.

935 Kent, D. V., Kjarsgaard, B. A., Gee, J. S., Muttoni, G., and Heaman, L. M., 2015, Tracking the Late Jurassic
936 apparent (or true) polar shift in U-Pb-dated kimberlites from cratonic North America (Superior Province of
937 Canada): Geochemistry, Geophysics, Geosystems, vol. 16, pp. 983–994, doi:10.1002/2015GC005734.

938 King, R. F., 1955, The remanent magnetism of artificially deposited sediments: Geophysical Journal International,
939 vol. 7, pp. 115–134, doi:10.1111/j.1365-246x.1955.tb06558.x.

940 Kirschvink, J. L., 1997, Evidence for a large-scale reorganization of early Cambrian continental masses by inertial
941 interchange true polar wander: Science, vol. 277, pp. 541–545, doi:10.1126/science.277.5325.541.

942 Kirschvink, J. L., Kopp, R. E., Raub, T. D., Baumgartner, C. T., and Holt, J. W., 2008, Rapid, precise, and
943 high-sensitivity acquisition of paleomagnetic and rock-magnetic data: Development of a low-noise automatic
944 sample changing system for superconducting rock magnetometers: Geochemistry, Geophysics, Geosystems, vol. 9,
945 pp. 1–18, doi:10.1029/2007gc001856.

946 Lan, Z., Huyskens, M. H., Lu, K., Li, X.-H., Zhang, G., Lu, D., and Yin, Q.-Z., 2020, Toward refining the onset age
947 of Sturtian glaciation in South China: Precambrian Research, vol. 338, p. 105,555,
948 doi:10.1016/j.precamres.2019.105555.

Lan, Z., Li, X.-H., Zhu, M., Zhang, Q., and Li, Q.-L., 2015, Revisiting the Liantuo Formation in Yangtze Block, South China: SIMS U-Pb zircon age constraints and regional and global significance: Precambrian Research, vol. 263, pp. 123–141, doi:10.1016/j.precamres.2015.03.012.

Li, J., Dong, S., Zhang, Y., Zhao, G., Johnston, S. T., Cui, J., and Xin, Y., 2016a, New insights into Phanerozoic tectonics of south China: Part 1, polyphase deformation in the Jiuling and Lianyunshan domains of the central Jiangnan Orogen: Journal of Geophysical Research: Solid Earth, vol. 121, pp. 3048–3080, doi:10.1002/2015jb012778.

Li, L., Lin, S., Xing, G., Davis, D. W., Jiang, Y., Davis, W., and Zhang, Y., 2016b, Ca. 830 Ma back-arc type volcanic rocks in the eastern part of the Jiangnan orogen: Implications for the Neoproterozoic tectonic evolution of South China Block: Precambrian Research, vol. 275, pp. 209–224, doi:10.1016/j.precamres.2016.01.016.

Li, X.-H., Li, W.-X., Li, Z.-X., Lo, C.-H., Wang, J., Ye, M.-F., and Yang, Y.-H., 2009, Amalgamation between the Yangtze and Cathaysia Blocks in South China: Constraints from SHRIMP U–Pb zircon ages, geochemistry and Nd–Hf isotopes of the Shuangxiwu volcanic rocks: Precambrian Research, vol. 174, pp. 117–128, doi:10.1016/j.precamres.2009.07.004.

Li, Z., Li, X., Kinny, P., Wang, J., Zhang, S., and Zhou, H., 2003, Geochronology of Neoproterozoic syn-rift magmatism in the Yangtze Craton, South China and correlations with other continents: evidence for a mantle superplume that broke up Rodinia: Precambrian Research, vol. 122, pp. 85–109, doi:10.1016/S0301-9268(02)00208-5.

Li, Z. X., Bogdanova, S. V., Collins, A. S., Davidson, A., Waele, B. D., Ernst, R. E., Fitzsimons, I. C. W., Fuck, R. A., Gladkochub, D. P., Jacobs, J., Karlstrom, K. E., Lu, S., Natapov, L. M., Pease, V., Pisarevsky, S. A., Thrane, K., and Vernikovsky, V., 2008, Assembly, configuration, and break-up history of Rodinia: a synthesis: Precambrian Research, vol. 160, pp. 179–210, doi:10.1016/j.precamres.2007.04.021.

Li, Z.-X. and Evans, D. A. D., 2011, Late Neoproterozoic 40° intraplate rotation within Australia allows for a tighter-fitting and longer-lasting Rodinia: Geology, vol. 39, pp. 39–42, doi:10.1130/g31461.1.

Li, Z. X., Evans, D. A. D., and Zhang, S., 2004, A 90° spin on Rodinia: possible causal links between the Neoproterozoic supercontinent, superplume, true polar wander and low-latitude glaciation: Earth and Planetary Science Letters, vol. 220, pp. 409–421, doi:10.1016/S0012-821X(04)00064-0.

Li, Z.-X., Li, X.-h., Zhou, H., and Kinny, P. D., 2002, Grenvillian continental collision in south China: New SHRIMP U-Pb zircon results and implications for the configuration of Rodinia: Geology, vol. 30, pp. 163–166, doi:10.1130/0091-7613(2002)030⟨0163:gccisc⟩2.0.co;2.

Li, Z.-X., Zhang, L., and Powell, C. M., 1995, South China in Rodinia: Part of the missing link between Australia–East Antarctica and Laurentia?: Geology, vol. 23, pp. 407–410, doi:10.1130/0091-7613(1995)023⟨0407:scirpo⟩2.3.co;2.

Lin, M., Peng, S., Jiang, X., Polat, A., Kusky, T., Wang, Q., and Deng, H., 2016, Geochemistry, petrogenesis and tectonic setting of Neoproterozoic mafic-ultramafic rocks from the western Jiangnan orogen, South China: Gondwana Research, vol. 35, pp. 338–356, doi:10.1016/j.gr.2015.05.015.

Ma, G., Li, H., Zhang, Z., et al., 1984, An investigation of the age limits of the Sinian System in South China: Bulletin of Yichang Institute of Geology and Mineral Resources, vol. 8, pp. 1–29.

Ma, H., Wang, Y., Huang, Y., and Xie, Y., 2019, Three-stage Mesozoic intracontinental tectonic evolution of South China recorded in an overprinted basin: evidence from stratigraphy and detrital zircon U-Pb dating: Geological Magazine, vol. 156, pp. 2085–2103, doi:10.1017/s0016756819000451.

Macdonald, F. A., Schmitz, M. D., Crowley, J. L., Roots, C. F., Jones, D. S., Maloof, A. C., Strauss, J. V., Cohen, P. A., Johnston, D. T., and Schrag, D. P., 2010, Calibrating the Cryogenian: Science, vol. 327, pp. 1241–1243, doi:10.1126/science.1183325.

MacLennan, S. A., Park, Y., Swanson-Hysell, N. L., Maloof, A. C., Schoene, B., Gebreslassie, M., Antilla, E., Tesema, T., Alene, M., and Haileab, B., 2018, The arc of the Snowball: U-Pb dates constrain the Islay anomaly and the initiation of the Sturtian glaciation: Geology, vol. 46, pp. 539–542, doi:10.1130/G40171.1.

Maloof, A. C., Halverson, G. P., Kirschvink, J. L., Schrag, D. P., Weiss, B. P., and Hoffman, P. F., 2006, Combined paleomagnetic, isotopic, and stratigraphic evidence for true polar wander from the Neoproterozoic Akademikerbreen Group, Svalbard, Norway: GSA Bulletin, vol. 118, pp. 1099–1124, doi:10.1130/B25892.1.

Matsuyama, I., Mitrovica, J. X., Daradich, A., and Gomez, N., 2010, The rotational stability of a triaxial ice-age Earth: Journal of Geophysical Research, vol. 115, doi:10.1029/2009jb006564.

Matsuyama, I., Nimmo, F., and Mitrovica, J. X., 2014, Planetary reorientation: Annual Review of Earth and Planetary Sciences, vol. 42, pp. 605–634, doi:10.1146/annurev-earth-060313-054724.

Mattinson, J. M., 2005, Zircon U-Pb chemical abrasion ("CA-TIMS") method: Combined annealing and multi-step partial dissolution analysis for improved precision and accuracy of zircon ages: Chemical Geology, vol. 220, pp. 47–66, doi:10.1016/j.chemgeo.2005.03.011.

McCabe, C. and Elmore, R. D., 1989, The occurrence and origin of Late Paleozoic remagnetization in the sedimentary rocks of North America: Reviews of Geophysics, vol. 27, p. 471, doi:10.1029/rg027i004p00471.

Meert, J. G., der Voo, R. V., Powell, C. M., Li, Z.-X., McElhinny, M. W., Chen, Z., and Symons, D. T. A., 1993, A plate-tectonic speed limit?: Nature, vol. 363, pp. 216–217, doi:10.1038/363216a0.

Meert, J. G., Pandit, M. K., and Kamenov, G. D., 2013, Further geochronological and paleomagnetic constraints on Malani (and pre-Malani) magmatism in NW India: Tectonophysics, vol. 608, pp. 1254–1267, doi:10.1016/j.tecto.2013.06.019.

Merdith, A. S., Collins, A. S., Williams, S. E., Pisarevsky, S., Foden, J. D., Archibald, D. B., Blades, M. L., Alessio, B. L., Armistead, S., Plavsa, D., and et al., 2017, A full-plate global reconstruction of the Neoproterozoic: Gondwana Research, vol. 50, pp. 84–134, doi:10.1016/j.gr.2017.04.001.

Meyers, S. R., Siewert, S. E., Singer, B. S., Sageman, B. B., Condon, D. J., Obradovich, J. D., Jicha, B. R., and Sawyer, D. A., 2012, Intercalibration of radioisotopic and astrochronologic time scales for the Cenomanian-Turonian boundary interval, Western Interior Basin, USA: Geology, vol. 40, pp. 7–10, doi:10.1130/g32261.1.

Michalski, K., Lewandowski, M., and Manby, G., 2011, New palaeomagnetic, petrographic and $^{40}Ar/^{39}Ar$ data to test palaeogeographic reconstructions of Caledonide Svalbard: Geological Magazine, vol. 149, pp. 696–721, doi:10.1017/s0016756811000835.

Mitrovica, J. X., Wahr, J., Matsuyama, I., and Paulson, A., 2005, The rotational stability of an ice-age earth: Geophysical Journal International, vol. 161, pp. 491–506, doi:10.1111/j.1365-246x.2005.02609.x.

Mound, J. E., Mitrovica, J. X., Evans, D. A. D., and Kirschvink, J. L., 1999, A sea-level test for inertial interchange true polar wander events: Geophysical Journal International, vol. 136, pp. F5–F10, doi:10.1046/j.1365-246x.1999.00791.x.

Niu, J., Li, Z.-X., and Zhu, W., 2016, Palaeomagnetism and geochronology of mid-Neoproterozoic Yanbian dykes, South China: implications for a c. 820–800 Ma true polar wander event and the reconstruction of Rodinia: Geological Society, London, Special Publications, vol. 424, pp. 191–211, doi:10.1144/SP424.11.

ParÃ©s, J. M., 2015, Sixty years of anisotropy of magnetic susceptibility in deformed sedimentary rocks: Frontiers in Earth Science, vol. 3, doi:10.3389/feart.2015.00004.

Parés, J. M., van der Pluijm, B. A., and Dinarès-Turell, J., 1999, Evolution of magnetic fabrics during incipient deformation of mudrocks (Pyrenees, northern Spain): Tectonophysics, vol. 307, pp. 1–14, doi:10.1016/s0040-1951(99)00115-8.

1036 Park, Y., Swanson-Hysell, N. L., MacLennan, S. A., Maloof, A. C., Gebreslassie, M., Tremblay, M. M., Schoene, B.,
1037 Alene, M., Anttila, E. S., Tesema, T., and Haileab, B., 2020, The lead-up to the Sturtian Snowball Earth:
1038 Neoproterozoic chemostratigraphy time-calibrated by the Tambien Group of Ethiopia: GSA Bulletin, vol. 132,
1039 pp. 1119–1149, doi:10.1130/b35178.1.

1040 Pi, D.-H. and Jiang, S.-Y., 2016, U-Pb dating of zircons from tuff layer, sandstone and tillite samples in the
1041 uppermost Liantuo Formation and the lowermost Nantuo Formation in Three Gorges area, South China:
1042 Chemie der Erde - Geochemistry, vol. 76, pp. 103 – 109, doi:10.1016/j.chemer.2015.12.003.

1043 Pisarevsky, S. A., Gladkochub, D. P., Konstantinov, K. M., Mazukabzov, A. M., Stanevich, A. M., Murphy, J. B.,
1044 Tait, J. A., Donskaya, T. V., and Konstantinov, I. K., 2013, Paleomagnetism of Cryogenian Kitoi mafic dykes in
1045 South Siberia: Implications for Neoproterozoic paleogeography: Precambrian Research, vol. 231, pp. 372–382,
1046 doi:10.1016/j.precamres.2013.04.007.

1047 Pisarevsky, S. A., Wingate, M. T. D., Stevens, M. K., and Haines, P. W., 2007, Palaeomagnetic results from the
1048 Lancer 1 stratigraphic drillhole, Officer Basin, Western Australia, and implications for Rodinia reconstructions:
1049 Australian Journal of Earth Sciences, vol. 54, pp. 561–572, doi:10.1080/08120090701188962.

1050 Qi, L., Cawood, P. A., Xu, Y., Du, Y., Zhang, H., and Zhang, Z., 2020, Linking South China to North India from
1051 the late Tonian to Ediacaran: Constraints from the Cathaysia Block: Precambrian Research, p. 105898,
1052 doi:10.1016/j.precamres.2020.105898.

1053 Qi, L., Xu, Y., Cawood, P. A., Wang, W., and Du, Y., 2019, Implications of 770 Ma rhyolitic tuffs, eastern South
1054 China Craton in constraining the tectonic setting of the Nanhua Basin: Lithos, vol. 324-325, pp. 842–858,
1055 doi:10.1016/j.lithos.2018.12.004.

1056 Ricard, Y., Spada, G., and Sabadini, R., 1993, Polar wandering of a dynamic earth: Geophysical Journal
1057 International, vol. 113, pp. 284–298, doi:10.1111/j.1365-246x.1993.tb00888.x.

1058 Sdrolias, M. and Müller, R. D., 2006, Controls on back-arc basin formation: Geochemistry, Geophysics, Geosystems,
1059 vol. 7, pp. 1–40, doi:10.1029/2005gc001090.

1060 Shen, Z., Fang, D., Wang, P., Tan, X., and Wang, Z., 1999, Paleomagnetism of early Triassic Daye Formation and
1061 its tectonic implications: Chinese Science Bulletin, vol. 44, pp. 412–418, doi:10.1007/bf02977877.

1062 Spada, G., Ricard, Y., and Sabadini, R., 1992, Excitation of true polar wander by subduction: Nature, vol. 360, pp.
1063 452–454, doi:10.1038/360452a0.

1064 Steinberger, B. and O'Connell, R. J., 1997, Changes of the Earth's rotation axis owing to advection of mantle
1065 density heterogeneities: Nature, vol. 387, pp. 169–173, doi:10.1038/387169a0.

1066 Steinberger, B. and Torsvik, T. H., 2008, Absolute plate motions and true polar wander in the absence of hotspot
1067 tracks: Nature, vol. 452, pp. 620–623, doi:10.1038/nature06824.

1068 Steinberger, B. and Torsvik, T. H., 2010, Toward an explanation for the present and past locations of the poles:
1069 Geochemistry, Geophysics, Geosystems, vol. 11, pp. 1–19, doi:10.1029/2009gc002889.

1070 Swanson-Hysell, N. L., Maloof, A. C., Condon, D. J., Jenkin, G. R., Alene, M., Tremblay, M. M., Tesema, T.,
1071 Rooney, A. D., and Haileab, B., 2015, Stratigraphy and geochronology of the Tambien Group, Ethiopia: evidence
1072 for globally synchronous carbon isotope change in the Neoproterozoic: Geology, vol. 43, pp. 323–326,
1073 doi:10.1130/G36347.1.

1074 Swanson-Hysell, N. L., Maloof, A. C., Kirschvink, J. L., Evans, D. A. D., Halverson, G. P., and Hurtgen, M. T.,
1075 2012, Constraints on Neoproterozoic paleogeography and Paleozoic orogenesis from paleomagnetic records of the
1076 Bitter Springs Formation, Amadeus Basin, central Australia: American Journal of Science, vol. 312, pp. 817–884,
1077 doi:10.2475/08.2012.01.

Swanson-Hysell, N. L., Vaughan, A. A., Mustain, M. R., and Asp, K. E., 2014, Confirmation of progressive plate motion during the Midcontinent Rift's early magmatic stage from the Osler Volcanic Group, Ontario, Canada: Geochemistry, Geophysics, Geosystems, vol. 15, pp. 2039–2047, doi:10.1002/2013GC005180.

Swanson-Hysell, N. L., Fairchild, L. M., and Slotznick, S. P., 2019, Primary and secondary red bed magnetization constrained by fluvial intraclasts: Journal of Geophysical Research: Solid Earth, vol. 124, pp. 4276–4289, doi:10.1029/2018jb017067.

Tauxe, L., 2005, Inclination flattening and the geocentric axial dipole hypothesis: Earth and Planetary Science Letters, vol. 233, pp. 247 – 261, doi:10.1016/j.epsl.2005.01.027.

Tauxe, L. and Kent, D. V., 1984, Properties of a detrital remanence carried by haematite from study of modern river deposits and laboratory redeposition experiments: Geophysical Journal International, vol. 76, pp. 543–561, doi:10.1111/j.1365-246X.1984.tb01909.x.

Tauxe, L., Shaar, R., Jonestrask, L., Swanson-Hysell, N. L., Minnett, R., Koppers, A. A. P., Constable, C. G., Jarboe, N., Gaastra, K., and Fairchild, L., 2016, PmagPy: Software package for paleomagnetic data analysis and a bridge to the Magnetics Information Consortium (MagIC) Database: Geochemistry, Geophysics, Geosystems, vol. 17, pp. 2450–2463, doi:10.1002/2016gc006307.

Tauxe, L. and Watson, G., 1994, The fold test: an eigen analysis approach: Earth and Planetary Science Letters, vol. 122, pp. 331–341, doi:10.1016/0012-821x(94)90006-x.

Tohver, E., Weil, A., Solum, J., and Hall, C., 2008, Direct dating of carbonate remagnetization by $^{40}Ar/^{39}Ar$ analysis of the smectite–illite transformation: Earth and Planetary Science Letters, vol. 274, pp. 524–530, doi:10.1016/j.epsl.2008.08.002.

Torsvik, T. H. and Cocks, L. R. M., 2016, Earth History and Palaeogeography: Cambridge University Press, doi:10.1017/9781316225523.

Torsvik, T. H., Van der Voo, R., Preeden, U., Mac Niocaill, C., Steinberger, B., Doubrovine, P. V., van Hinsbergen, D. J., Domeier, M., Gaina, C., Tohver, E., Meert, J. G., McCausland, P. J. A., and Cocks, L. R. M., 2012, Phanerozoic polar wander, palaeogeography and dynamics: Earth-Science Reviews, vol. 114, pp. 325–368, doi:10.1016/j.earscirev.2012.06.007.

Tsai, V. C. and Stevenson, D. J., 2007, Theoretical constraints on true polar wander: Journal of Geophysical Research, vol. 112, doi:10.1029/2005jb003923.

Van Der Voo, R. and Torsvik, T. H., 2012, The history of remagnetization of sedimentary rocks: deceptions, developments and discoveries: Geological Society, London, Special Publications, vol. 371, pp. 23–53, doi:10.1144/sp371.2.

van Hinsbergen, D. J. J., Steinberger, B., Doubrovine, P. V., and Gassmöller, R., 2011, Acceleration and deceleration of India-Asia convergence since the Cretaceous: Roles of mantle plumes and continental collision: Journal of Geophysical Research, vol. 116, doi:10.1029/2010jb008051.

Veevers, J. J. and Eittreim, S. L., 1988, Reconstruction of Antarctica and Australia at breakup (95 ± 5 Ma) and before rifting (160 Ma): Australian Journal of Earth Sciences, vol. 35, pp. 355–362, doi:10.1080/08120098808729453.

Wang, J. and Li, Z.-X., 2003, History of Neoproterozoic rift basins in South China: implications for Rodinia break-up: Precambrian Research, vol. 122, pp. 141 – 158, doi:10.1016/S0301-9268(02)00209-7.

Wang, M., Dai, C., Chen, J., Wang, X., and Ma, H., 2016a, Neoproterozoic geochronologic framework of magmatism in Fanjingshan area and its tectonic implications: Geology in China, vol. 43, pp. 843–856.

Wang, M., Dai, C., Wang, X., Ma, H., Peng, C., and Yang, K., 2012, Sedimentation age of the Fanjingshan Group in East Guizhou Province: evidence from in-situ zircon LA-ICP-MS U-Pb dating: Acta Petrologica et Mineralogica, vol. 31, pp. 843–857.

Wang, T., Zhang, S., and Ramezani, J., 2016b, Age recalibration of the Xiaofeng dykes, South China, and its implications for true polar wander at ∼820 Ma: Acta Geologica Sinica - English Edition, vol. 90, p. 47, doi:10.1111/1755-6724.12878.

Wang, W., Zhao, J.-H., Zhou, M.-F., Yang, S.-H., and Chen, F.-K., 2014, Neoproterozoic mafic-ultramafic intrusions from the Fanjingshan Region, South China: Implications for subduction-related magmatism in the Jiangnan Fold Belt: The Journal of Geology, vol. 122, pp. 455–473, doi:10.1086/676596.

Wei, Y., Peng, S., Jiang, X., Peng, Z., Peng, L., Li, Z., Zhou, P., and Zeng, X., 2012, SHRIMP zircon U-Pb ages and geochemical characteristics of the Neoproterozoic granitoids in the Huangling anticline and its tectonic setting: Journal of Earth Science, vol. 23, pp. 659–676, doi:10.1007/s12583-012-0284-z.

Weil, A. B., Geissman, J. W., and Ashby, J. M., 2006, A new paleomagnetic pole for the Neoproterozoic Uinta Mountain supergroup, Central Rocky Mountain States, USA: Precambrian Research, vol. 147, pp. 234–259, doi:10.1016/j.precamres.2006.01.017.

Wingate, M. T. D. and Giddings, J. W., 2000, Age and palaeomagnetism of the Mundine Well dyke swarm, Western Australia: implications for an Australia–Laurentia connection at 755 Ma: Precambrian Research, vol. 100, pp. 335–357, doi:10.1016/S0301-9268(99)00080-7.

Xian, H., Zhang, S., Li, H., Yang, T., and Wu, H., 2020, Geochronological and palaeomagnetic investigation of the Madiyi Formation, lower Banxi Group, South China: Implications for Rodinia reconstruction: Precambrian Research, vol. 336, pp. 1–13, doi:10.1016/j.precamres.2019.105494.

Xiong, G., Wang, J., Wu, H., Zhang, H., Yu, Q., Yan, J., Jiang, X., Cui, X., and Wang, Z., 2014, Trace element and REE geochemistry of the Ediacaran Doushantuo Formation from Fanjingshan area, northeast Guizhou province, China: Carbonates and Evaporites, vol. 29, pp. 363–394, doi:10.1007/s13146-014-0217-2.

Yan, C., Shu, L., Faure, M., Chen, Y., and Huang, R., 2019, Time constraints on the closure of the Paleo-South China Ocean and the Neoproterozoic assembly of the Yangtze and Cathaysia blocks: Insight from new detrital zircon analyses: Gondwana Research, vol. 73, pp. 175–189, doi:10.1016/j.gr.2019.03.018.

Yao, J., Cawood, P. A., Shu, L., and Zhao, G., 2019, Jiangnan Orogen, South China: A ∼970-820 Ma Rodinia margin accretionary belt: Earth-Science Reviews, vol. 196, p. 102,872, doi:10.1016/j.earscirev.2019.05.016.

Zahirovic, S., Müller, R. D., Seton, M., and Flament, N., 2015, Tectonic speed limits from plate kinematic reconstructions: Earth and Planetary Science Letters, vol. 418, pp. 40–52, doi:10.1016/j.epsl.2015.02.037.

Zahirovic, S., Müller, R. D., Seton, M., Flament, N., Gurnis, M., and Whittaker, J., 2012, Insights on the kinematics of the India-Eurasia collision from global geodynamic models: Geochemistry, Geophysics, Geosystems, vol. 13, pp. 1–25, doi:10.1029/2011gc003883.

Zhang, J., Ye, T., Dai, Y., Chen, J., Zhang, H., Dai, C., Yuan, G., and Jiang, K., 2019, Provenance and tectonic setting transition as recorded in the Neoproterozoic strata, western Jiangnan Orogen: Implications for South China within Rodinia: Geoscience Frontiers, vol. 10, pp. 1823–1839, doi:10.1016/j.gsf.2018.10.009.

Zhang, S., Evans, D. A., Li, H., Wu, H., Jiang, G., Dong, J., Zhao, Q., Raub, T. D., and Yang, T., 2013, Paleomagnetism of the late Cryogenian Nantuo Formation and paleogeographic implications for the South China Block: Journal of Asian Earth Sciences, vol. 72, pp. 164–177, doi:10.1016/j.jseaes.2012.11.022.

Zhao, J.-H., Zhou, M.-F., Yan, D.-P., Zheng, J.-P., and Li, J.-W., 2011, Reappraisal of the ages of Neoproterozoic strata in South China: No connection with the Grenvillian orogeny: Geology, vol. 39, pp. 299–302, doi:10.1130/g31701.1.

1162 Zheng, L., Yang, Z., Tong, Y., and Yuan, W., 2010, Magnetostratigraphic constraints on two-stage eruptions of the
1163 Emeishan continental flood basalts: Geochemistry, Geophysics, Geosystems, vol. 11, pp. 1–19,
1164 doi:10.1029/2010gc003267.

1165 Zhou, J.-C., Wang, X.-L., and Qiu, J.-S., 2009, Geochronology of Neoproterozoic mafic rocks and sandstones from
1166 northeastern Guizhou, South China: Coeval arc magmatism and sedimentation: Precambrian Research, vol. 170,
1167 pp. 27–42, doi:10.1016/j.precamres.2008.11.002.

1168 Zhu, R., Potts, R., Pan, Y., Lü, L., Yao, H., Deng, C., and Qin, H., 2008, Paleomagnetism of the Yuanmou Basin
1169 near the southeastern margin of the Tibetan Plateau and its constraints on late Neogene sedimentation and
1170 tectonic rotation: Earth and Planetary Science Letters, vol. 272, pp. 97–104, doi:10.1016/j.epsl.2008.04.016.